Journal of the American Society of NEPHROLOGY

JASN

Reduced renal methylarginine metabolism protects against progressive kidney damage

Journal:	*Journal of the American Society of Nephrology*
Manuscript ID:	JASN-2014-03-0280.R2
Manuscript Type:	Original Article - Basic Research
Date Submitted by the Author:	16-Feb-2015
Complete List of Authors:	Tomlinson, James; Medical Research Council Clinical Sciences Centre, Imperial College, Nitric Oxide Signalling Caplin, Ben; UCL Medical School Royal Free, Centre for Nephrology Boruc, Olga; Medical Research Council Clinical Sciences Centre, Imperial College, Nitric Oxide Signalling Bruce-Cobbold, Claire; Medical Research Council Clinical Sciences Centre, Imperial College, Nitric Oxide Signalling Cutillas, Pedro; Queen Mary, University of London, Centre for Haemato-Oncology Dorman, Dirk; Medical Research Council Clinical Sciences Centre, Imperial College, Microscopy Faull, Peter; Medical Research Council Clinical Sciences Centre, Imperial College, Proteomics Grossman, Rebecca; UCL Medical School Royal Free, Centre for Nephrology Khadayate, Sanjay; Medical Research Council Clinical Sciences Centre, Imperial College, Bioinformatics Mas, Valeria; University of Virginia, Department of Surgery; Nitsch, Dorothea; London School of Hygiene & Tropical Medicine, Non Communicable Disease Epidemiology Wang, Zhen; Medical Research Council Clinical Sciences Centre, Imperial College, Nitric Oxide Signalling Norman, Jill; UCL Medical School Royal Free, Centre for Nephrology Wilcox, Christopher; Georgetown University Hospital, Medicine - Division of Nephrology and Hypertension Wheeler, David; Royal Free Hospital, Centre for Nephrology, Royal Free and University College Medical School; Leiper, James; Medical Research Council Clinical Sciences Centre, Imperial College, Nitric Oxide Signalling
Keywords:	nitric oxide, chronic renal failure, fibrosis, Pathophysiology of Renal Disease and Progression, proximal tubule, transgenic mouse

SCHOLARONE™
Manuscripts

ScholarOne support: 888-503-1050

For Peer Review

Reduced Renal Methylarginine Metabolism Protects against Progressive Kidney Damage

Tomlinson JAP[1§], Caplin B[2], Boruc O[1], Bruce-Cobbold C[1], Cutillas P[1], Dormann D[1], Faull P[1], Grossman RC[2], Khadayate S[1], Mas VR[4], Nitsch D[5], Wang Z[1], Norman J[2], Wilcox CS[3], Wheeler DC[2], Leiper J[1]

[1]Medical Research Council Clinical Sciences Centre, Imperial College, London, United Kingdom
[2]Centre for Nephrology, UCL Medical School Royal Free, London, United Kingdom
[3]Hypertension, Kidney and Vascular Research Center, Georgetown University, Washington, DC, United States
[4]Translational Genomics Transplant Laboratory, Transplant Division, Department of Surgery, University of Virginia, Charlottesville, Virginia, United States
[5]Department of Non-communicable Disease Epidemiology, London School of Hygiene and Tropical Medicine, London, United Kingdom

Running title: Methylarginines in Kidney Disease

Abstract word count: 248

Text word count: 2972

[§]Corresponding author:
Dr James Tomlinson
Medical Research Council Clinical Sciences Centre, Imperial College, Hammersmith Hospital Campus, DuCane Road, London, W12 0NN, United Kingdom
Phone: +442083838405
Fax: +442083834318

Email: j.tomlinson@imperial.ac.uk

For Peer Review

Abstract

Nitric oxide (NO) production is diminished in many patients with cardiovascular and renal disease. Asymmetric dimethylarginine (ADMA) is an endogenous inhibitor of NO synthesis, and elevated plasma levels of ADMA are associated with poor outcomes. Dimethylarginine dimethylaminohydrolase-1 (*DDAH1*) is a methylarginine-metabolizing enzyme that reduces ADMA levels. We reported previously that a *DDAH1* gene variant associated with increased renal *DDAH1* mRNA transcription and lower plasma ADMA levels, but counter-intuitively, a *steeper* rate of renal function decline. Here, we test the hypothesis that reduced renal-specific ADMA metabolism protects against progressive renal damage.

Renal *DDAH1* is expressed predominately within the proximal tubule. A novel proximal tubule-specific *Ddah1* knockout ($Ddah1^{PT-/-}$) mouse demonstrated tubular cell accumulation of ADMA and lower NO concentrations, but unaltered plasma ADMA concentrations. $Ddah1^{PT-/-}$ mice were protected from reduced kidney tissue mass, collagen deposition, and profibrotic cytokine expression in two independent renal injury models, folate nephropathy and unilateral ureteric obstruction. Furthermore, a study of two independent kidney transplant cohorts revealed higher levels of human renal allograft methylarginine-metabolizing enzyme gene expression associating with steeper function decline. Additionally, we report an association between *DDAH1* expression, NO activity, and uromodulin expression supported by data from both animal and human studies, raising the possibility that kidney *DDAH1* expression exacerbates renal injury through uromodulin-related mechanisms.

Together, these data demonstrate that reduced renal tubular ADMA metabolism protects against progressive kidney function decline. Thus, circulating ADMA may be an imprecise marker of renal methylarginine metabolism and therapeutic ADMA reduction may even be deleterious to kidney function.

For Peer Review

Introduction

Chronic kidney disease (CKD) poses an increasing global disease burden and contributes to cardiovascular disease (CVD), which is the leading cause of death worldwide. [1,2] CKD is associated with reduced bioavailability of nitric oxide (NO), which is required to maintain normal vascular and kidney function. [3,4] Asymmetric dimethylarginine (ADMA) is released into the cytoplasm during normal protein turnover and competes with L-arginine binding at the active site of nitric oxide synthase (NOS) to block NO synthesis. The methylarginine-metabolising enzymes (MAMEs); dimethylarginine dimethylaminohydrolase isoforms 1 and 2 (DDAH 1 and 2) and alanine-glyoxylate aminotransferase-2 (AGXT2), [5] metabolize ADMA and other methylarginines to inactive products. Thus, MAMEs represent alternative pathways of endogenous NO regulation. [6]

The kidney expresses all MAME and NOS isoforms in a cell-specific distribution [5,7,8] thereby providing the means for intricate, cell type-specific control of NO bioavailability. Renal NO regulates hemodynamics, [9] afferent arteriolar vascular reactivity, [10] glomerular filtration, [11] tubular reabsorption and solute excretion. [8,12] Specifically, the proximal tubule (PT) is the principal renal cell type expressing the enzyme with the greatest activity for metabolism of ADMA, DDAH1, [7,13] although how this influences tubular reabsorption and response to injury through NO-ADMA regulation is unclear. Human studies demonstrate arterio-venous ADMA gradients across the kidney, which represent a large proportion of total body ADMA clearance through enzymatic metabolism and urinary excretion. [14] Consequently, plasma ADMA levels rise with declining kidney function, as demonstrated by Vallance et al with an early report of elevated plasma ADMA, lower NO and vascular dysfunction in patients with end-stage renal disease (ESRD). [15]

Raised circulating ADMA is a powerful predictor of progressive CVD and CKD, independent of eGFR and other traditional risk factors. [16-20] Since plasma ADMA increases with declining kidney function, the direction of causality is difficult to resolve by correlation alone. Although increased plasma ADMA levels may correlate with reduced total body NO bioavailability, they do not necessarily reflect the balance of NOS inhibition within the renal interstitium during progressive CKD. Our published data suggests that lower plasma ADMA does not necessarily protect against renal function decline and

For Peer Review

that increased *DDAH1* activity limited to the kidney may in fact be harmful. Thus, we reported a non-coding *DDAH1* variant (rs17384213) that was associated with higher renal *DDAH1* mRNA expression and lower plasma ADMA concentrations but counter-intuitively, this correlated with a *faster* rate of eGFR decline in two independent cohorts of patients with CKD. [21] It is possible that competitive inhibition of NOS by ADMA plays both protective and pathogenic roles, [6] determined by factors such as disease site, time-course and magnitude of response.

In light of these uncertainties, it is clearly important to define the role of PT-specific *DDAH1* in CKD progression. We hypothesised that reduced renal *DDAH1* activity protects against renal function decline, independent of circulating NO and ADMA.

Results

Proximal tubule (PT) specific gene targeting

The proximal tubule (PT) is the principal renal cell type to express *DDAH1* ([7,13] and Figure 1). Conditional proximal-tubule specific gene manipulation was achieved using the *KAP2iCre* gene construct. [22] Regulatory elements of the KAP (kidney androgen-regulated protein) promoter and angiotensinogen genes confer highly PT-specific, codon-optimised Cre (iCre) expression in response to androgen stimulation.

Two double transgenic mouse strains were created, both possessing the *KAP2iCre* gene along with either; *ROSA26eYFP* – a reporter strain designed to confirm PT-specific gene manipulation (loxP sites flank a *YFP* STOP codon; Figure 2A), or floxed *Ddah1* (loxP sites flank exon 1 of *Ddah1* which encodes the initiating methionine residue and the first 100 amino acids of the protein; Figure 2D). [23] In order to achieve temporal control over PT-specific KAP2iCre expression and gene disruption, only female mice were treated with exogenous testosterone and used for study.

YFP expression in female *KAP2iCre/ROSA26eYFP* reporter mice treated with testosterone was demonstrated using ImageStream analysis of isolated renal tubular cells (Figure 2B) and by renal tissue histology (Figure 2C). Mice not possessing the *KAP2iCre* transgene did not express *YFP*.

For Peer Review

PT-specific *Ddah1* deletion

The *Ddah1* gene was deleted after testosterone exposure in *KAP2iCre/Ddah1*-floxed mice ($Ddah1^{PT-/-}$) but not in *Ddah1*-floxed ($Ddah1^{fl/fl}$) controls (Figure 2E). Reduced *Ddah1* expression was clearly observed in the kidney where it exceeded 50% (Figure 2F; $p<0.05$). Non-significant reductions were detected in the liver and brain. Whole kidney lysate DDAH1 protein expression in $Ddah1^{PT-/-}$ mice was reduced by ~80% (Figure 2G; $p<0.001$) and enzymatic DDAH1 activity was reduced by ~70% (Figure 2H; $p<0.05$).

Downstream effects of PT-specific *Ddah1* deletion on MAs and NO

ADMA recovered from isolated renal tubules was almost 7-fold higher ($p<0.05$) and NOx was 2.5-fold lower ($p<0.05$) in $Ddah1^{PT-/-}$ mice versus $Ddah1^{fl/fl}$ controls (Figure 3A, B). The impact of PT-specific *Ddah1* deletion was restricted to tubular isolates and not evident in whole kidney tissue, plasma or urine, indicating tubule-specific ADMA-NO perturbation (Figure 3A-H). This was further demonstrated by an absence of baseline effects upon renal expression of alternative MAME isoforms and NOS enzymes (Figure 3I); systolic BP (Figure 3J); renal function according to plasma creatinine (Figure 3K) and urinary volumes (Figure 3L).

Effects of PT-specific *Ddah1* deletion on urine biochemistry

Urinary electrolytes, protein and amino acid concentrations were not significantly affected by PT-specific *Ddah1* deletion (Figure 4A-F). However, using a proteomic approach, significant effects of tubular *Ddah1* disruption upon a number of urinary peptides were observed under baseline conditions. Of 1057 peptides screened in $Ddah1^{PT-/-}$ and $Ddah1^{fl-/fl}$ mouse urine, relative concentrations of 82 peptides were significantly altered (Figure 5; $p<0.05$). Most significantly downregulated in $Ddah1^{PT-/-}$ mouse urine was uromodulin (UMOD), (8.5-fold lower in urine from $Ddah1^{PT-/-}$ mice compared to $Ddah1^{fl-/fl}$ controls) (Figure 5; $p=0.00042$ or $q=0.00083$). In addition, urinary Col1α1 was down-regulated 6.5-fold in $Ddah1^{PT-/-}$ mice ($p=0.0013$; $q=0.0017$) at baseline.

The effect of PT-specific *Ddah1* deletion in folate nephropathy

A single intra-peritoneal injection of folate induced an acute tubular injury in all mice, manifested by gross tubular dilatation, luminal casts and interstitial

For Peer Review

inflammatory cell infiltrates (Figure 6; see Supplementary Material for a full characterization of folate nephropathy in wild-type mice). At 12 weeks following folate, significant differences emerged between *Ddah1*$^{PT-/-}$ and *Ddah1*$^{fl-/fl}$ control mice. Renal collagen deposition was significantly lower in *Ddah1*$^{PT-/-}$ mice treated with folate compared to *Ddah1*$^{fl-/fl}$ controls (Figures 7 and 8; $p<0.05$). In addition, reduction in renal mass according to kidney:body weight ratios was significantly attenuated in *Ddah1*$^{PT-/-}$ versus *Ddah1*$^{fl-/fl}$ mice (Figure 7B; <0.01). Kidney tissue pro-fibrotic cytokine expression was 3 - 5 fold lower in *Ddah1*$^{PT-/-}$ mice (Figure 7C; Col1a2 $p<0.05$; TGFβ <0.01; ET-1 $p<0.05$). Furthermore at 12 weeks, *Ddah1*$^{PT-/-}$ mice were protected from other manifestations of advanced renal impairment such as hypertension (systolic BP; Figure 7D; $p<0.01$) and raised plasma creatinine (Figure 7E; $p<0.001$). There was a trend toward lower levels of proteinuria in *Ddah1*$^{PT-/-}$ mice although this did not reach statistical significance (Figure 7E; $p=0.21$).

The effect of PT-specific *Ddah1* deletion in unilateral ureteric obstructive (UUO) nephropathy

In order to confirm that the protection against fibrosis observed with PT-specific *Ddah1* deletion was not a phenomenon unique to folate toxicity, *Ddah1*$^{PT-/-}$ mice were exposed to a second renal injury model; unilateral ureteric obstruction (UUO). (See Supplementary Material for a detailed characterization of UUO nephropathy in wild-type mice).

At two weeks following UUO, severe tubulointerstitial disease was evident in kidney sections from obstructed kidneys, with gross tubular dilatation, epithelial cell flattening, parenchymal thinning and collagen deposition (Supplementary Material). When compared to *Ddah1*$^{fl/fl}$ controls, kidney tissue from *Ddah1*$^{PT-/-}$ mice exhibited reduced loss of renal mass ($p<0.05$) and collagen deposition ($p<0.05$; Figure 9A-C). Furthermore kidney tissue expression of pro-fibrotic genes Col1α2 and TGFβ was significantly lower in *Ddah1*$^{PT-/-}$ mice ($p<0.05$; Figure 9D).

Allograft MAME expression and eGFR decline in humans

To confirm laboratory findings described above, we measured kidney tissue MAME (*DDAH1* and *AGXT2*) transcript levels and eGFR decline in two independent human renal transplant cohorts (Table 1). In both the London and the Virginia cohort, there was a strong positive correlation between

For Peer Review

corrected *DDAH1* expression and corrected *AGXT2* expression (supplementary data). Therefore for further analysis of eGFR decline we used a composite methylarginine gene expression calculated from the geometric mean of the *DDAH1* and *AGXT2* expression. In both cohorts, higher MAME expression was associated with a steeper decline in eGFR over the one year following allograft biopsy (Table 2). Although there was an association between MAME expression and baseline eGFR in the Virginia cohort this did not reach statistical significance in the London subjects. The multilevel approach allows estimation of the association between gene expression and eGFR decline independent of the baseline eGFR as illustrated in Figure 10.

An association between kidney *DDAH1* expression, NO activity and UMOD

Given the findings of lower urinary UMOD peptide in proteomic analysis of *Ddah1*$^{PT-/-}$ mouse urine, we examined the association between *DDAH1* gene expression and urinary *UMOD* protein concentration in the London patient cohort. Although there was only a trend toward a positive correlation in the cohort as a whole, a significant association between *DDAH1* gene expression and urinary *UMOD* was observed when the analysis was restricted to recipients of live donor allografts (in order to minimise the impact of ischaemia and other confounding variables associated with deceased donor organs; Figure 11A; p=0.039).

To establish whether the positive correlation between renal DDAH1 activity and UMOD protein expression observed in the *Ddah1*$^{PT-/-}$ mouse and human cohort was NO-dependent, we performed a further *in vivo* study in wild-type mice receiving a non-selective nitric oxide synthase (NOS) inhibitor (L-NG-Nitroarginine Methyl Ester; L-NAME). Changes in renal UMOD protein expression were assessed. Following two weeks of L-NAME treatment (1mg/mL dissolved in drinking water – concentrations previously established to systemically inhibit NOS *in vivo* [24-26]), kidney tissue NOx (nitrites and nitrates) were reduced by 25% ($p<0.01$). Furthermore, UMOD protein expression was significantly reduced following L-NAME treatment; 40% in kidney tissue ($p<0.01$) and 30% in urine ($p<0.01$; Figure 11B-E).

For Peer Review

Discussion

We focussed this study on MAME activity limited to kidney tissue by exposing a novel transgenic mouse strain to two different forms of renal injury and examining renal biopsy and outcome data from two human cohorts. Our results lead us to conclude that *local* imbalances of the NO-ADMA-MAME axis may determine kidney function decline more reliably than circulating ADMA. Proximal tubule cell-specific *DDAH1* deletion was dissociated from baseline plasma ADMA and systemic BP. The observed protection against kidney collagen deposition and functional decline was therefore independent of systemic confounders and distinguishes a critical difference between local (protective) and systemic (harmful) effects of ADMA in renal function decline.

Data from two human renal transplant cohorts support the animal studies. Modeling renal function over time in the post-transplant period using laboratory values is not straightforward. Our estimates show substantial unexplained variation that was not significantly improved with addition of other clinical variables. Despite this, we detected an association between eGFR decline and increased MAME expression in both renal transplant cohorts. The relationship between the *DDAH1* and *AGXT2* enzymes is unclear but their relative expression was strongly correlated and a summary composite (geometric mean) of both the enzymes was used to demonstrate that raised kidney tissue MAME expression correlated with poorer outcomes in terms of eGFR.

Our findings suggest a re-analysis of previously published human observational data showing that elevated plasma ADMA was associated with progression of renal disease. [19,20,27] Interestingly, in the largest study of CKD patients to date, no association was observed between serum methylarginine levels and renal progression once baseline GFR was taken into account. [19] Previously, using a Mendelian randomisation approach (with less susceptibility to reverse causation and residual confounding), we reported a gene variant that conferred higher kidney tissue *DDAH1* mRNA expression, and associated with more rapid renal decline. [21]

Previously published rodent studies of kidney fibrosis have reported that *DDAH1* and NO are protective whilst ADMA is pathogenic, however significant study design issues limit their interpretation. ADMA or L-NAME infusion into

For Peer Review

mice exacerbated renal fibrosis but both raised SBP by approximately 60mmHg suggesting hypertensive injury, [28] whilst global *DDAH1* overexpression showed protection against fibrosis in angiotensin and surgical nephron-reduction models of CKD. [29,30] Genetic *DDAH1* overexpression decreases circulating ADMA and introduces unmeasured effects upon normal regulatory mechanisms. Furthermore, *DDAH1* overexpression occurs indiscriminately in cell types that do not normally express *DDAH1,* but play significant roles in inflammation and fibrosis (eg. macrophages). Here, PT-specific *DDAH1* gene deletion raises ADMA and reduces NO availability only within tubules and provides protection against fibrosis and functional decline in two different models of nephropathy.

Proteomic urinalysis data in *Ddah1*$^{PT-/-}$ mice suggests that reduced tubular NO activity may confer protection against progressive fibrosis in folate and UUO nephropathy through reduced expression of collagen and UMOD proteins. A stimulatory role of NO activity upon collagen deposition and wound healing in skin and tendon tissue has been shown in *in vitro* and *in vivo* studies using exogenous NO donors, [31] iNOS overexpression [32] and even dietary L-arginine supplementation. [33] Published literature confirms NO as a pleiotropic molecule in the kidney as well as other systems [34] with both protective and deleterious effects exerted by NO upon collagen deposition and fibrosis in renal disease. [35-39] What is clear is that maladaptive, pro-fibrotic responses to injury are at least in part, driven by cross-talk between high NO activity and fibrotic mediators such as TGFβ and matrix metalloproteases (MMPs) through SMAD signalling and other pathways. [37] Relevant to our own findings, pharmacological DDAH1 inhibition (causing reduced NO activity) has been demonstrated to reduce collagen deposition in a TGFβ and SMAD-dependent manner in a bleomycin model of pulmonary fibrosis. [40]

An association between urinary *UMOD* and renal *DDAH1* expression was identified in both the *Ddah1*$^{PT-/-}$ mouse and human cohort data. An 8.5-fold reduction of *UMOD* in *Ddah1*$^{PT-/-}$ suggests that functional changes in MAMEs and NO synthesis within the proximal tubule are communicated downstream along the nephron to the thick ascending limb, where *UMOD* is exclusively expressed. [41] A link between NO activity and UMOD expression was confirmed in wild-type mice exposed to a non-selective NOS inhibitor (L-NAME), which

For Peer Review

resulted in reduced UMOD protein expression in kidney tissue and urine. Interestingly, NO is known to exert regulatory control over two transcription factors; nuclear factor of activated T cells (NFAT) [42] and Oct-1, [43] both of which have consensus binding sites in the promoter region of *UMOD.* [44] These observations raise the possibility of direct regulation of UMOD expression by NO, a suggestion that certainly warrants further study. Genome-wide association studies (GWAS) identify a number of *UMOD* polymorphisms that associate with raised *UMOD* expression, hypertension, CKD and kidney function. [45] A recent report confirmed that common *UMOD* gene variants increase *UMOD* expression and that (salt-sensitive) hypertension and CKD progression may be induced through NKCC2 co-transporter stimulation. [46] In our study, reduced *DDAH1* metabolism of methylarginines (in the proximal tubule) correlates with lower *UMOD* expression downstream and consistent with published data, may in part explain the protective effect observed against kidney disease progression.

This study has several limitations. A minor degree of extra-renal (liver and brain) *DDAH1* gene deletion in the *Ddah1*$^{PT-/-}$ mouse was suggested using sensitive PCR-based assays although this did not reach a level of statistical significance in *DDAH1* mRNA transcription in these tissues. This may represent a constitutive leak of Cre expression autonomous of androgen stimulation, or Cre activation in response to even very low-levels of circulating testosterone in females. It is unlikely that such changes in neuronal or hepatic *DDAH1* activity, in the absence of altered BP or systemic ADMA, could influence renal fibrosis. It is known that off-target Cre expression and activity is widely under-reported. [47] Cre toxicity has been reported to cause cardiomyopathy, [48] brain development defects [49] and widespread apoptosis in embryos. [50] To our knowledge, there are no descriptions of Cre-toxicity relating to fibrosis and any effects to date suggest that Cre acts to disrupt normal cellular function or architecture rather than preserve it, as seen in the *Ddah1*$^{PT-/-}$ mouse. Other limitations such as relatively small patient sample numbers are counterbalanced by findings that are consistent across two very different experimental models of renal injury and human observational data examining gene expression and clinical outcomes in two independent cohorts.

For Peer Review

In conclusion, we demonstrate that a reduction in renal ADMA metabolism protects against renal function decline in the context of renal injury. Whether therapeutic reduction of circulating ADMA would improve CV outcomes at the same time as accelerating renal fibrosis requires further investigation. Our findings suggest that, at least in the kidney, non-selective ADMA reduction could be detrimental.

For Peer Review

Concise methods

Animal studies

Animal experiments and husbandry were performed under UK Home Office License after approval by the local ethics committee. The KAPiCre (KC) transgenic mouse on a C57B6 background was purchased from Jackson Laboratories (strain name: B6.Cg-Tg(Kap-cre)29066/2Sig/J). The ROSAYFP mouse (mixed background) was a kind gift from Professor Graham Williams (Imperial College, London). *DDAH1* floxed mice on a mixed background were previously developed and supplied by our group. LoxP sites flank exon 1 of *DDAH1* (exon 1 contains the initiating methionine codon and encodes the first 100 amino acids of *DDAH1* (approximately 35% of the total protein)). To achieve temporal activation of KC, female mice were treated with a subcutaneous testosterone pellet (Innovative Research of America, FL) for a minimum of ten days. Animals were placed in metabolic cages for a maximum of 24 hours and urine collected was centrifuged at 8,000 x g for 10 minutes, the supernatant stored at -80°C.

Invasive blood pressure (IBP) recording was performed under terminal (1%) isoflurane anaesthesia. A *'Mikro-Tip'* pressure transducer catheter (Millar Instruments, TX) placed into the carotid artery. Recordings were obtained using the Powerlab system with analysis on Chart software (both ADInstruments, Oxfordshire, UK).

Folate nephropathy. Mice received a single intra-peritoneal injection of folate (240μg/g) dissolved in 0.3M $NaHCO_3$ vehicle (20mg/mL) or vehicle control alone (both from Sigma, Dorset, UK). Mice were sacrificed by CO_2 narcosis and cervical dislocation at day 2, day 14 or day 84 (12 weeks). Blood collected by direct cardiac puncture was stored on ice before centrifugation at 8,000 x g to remove plasma. The right kidney was halved (sagittal plane) for histology, and quartered for future RNA and protein extraction while the left kidney was weighed. Samples were stored at -80°C.

Unilateral ureteric obstructive (UUO) nephropathy. Under isoflurane inhalation anaesthesia, mice were shaved, draped and positioned on a heat mat. In the supine position, a left flank incision exposed the left ureter and was ligated twice with 4-0 nylon sutures and transected. Following suture closure, animals received intramuscular diclofenac analgesia (Vetagesic) and

For Peer Review

recovered in heated chambers. Mice were sacrificed by cervical dislocation followed by organ harvesting at three time points; 1, 2 and 3 weeks.

L-NAME experiment. Female littermate wild-type C57BL/6 mice aged approximately 10 weeks old were randomly allocated to receive either plain deionized drinking water or the same water containing dissolved L-NG-Nitroarginine Methyl Ester (L-NAME; 1mg/mL, Enzo Life Sciences). n=8 in each group. Water was changed every three days and mice were sacrificed by CO_2 narcosis and cervical dislocation. Urine was collected for 24 hours prior to sacrifice and kidney tissue was harvested, snap frozen in liquid nitrogen and stored at -80°C before further analysis.

Renal tubule isolation. Mice were sacrificed by CO_2 narcosis and cervical dislocation, the abdominal aorta was ligated superior to the renal arteries and magnetic beads (Dynabeads M-450 Tosylactivated, Invitrogen, Paisley, UK) suspended in ice-cold HBSS were infused via an aortic catheter placed distally and kidney perfusion confirmed by rapid blanching. Kidneys were then dissected out, decapsulated and minced with a scalpel before incubation in collagenase (1mg/mL, Sigma, Dorset, UK) at 37°C for 30mins with agitation. The resulting homogenate was successively sieved through 100μ and 50μ pore sizes and fragments caught by the latter were resuspended in cold HBSS. Magnetic separation of glomerular and tubular fragments was confirmed by microscopic examination (bead entrapment visible within glomerular capillary loops). Purified tubules were pelleted by centrifugation at 1000 x g and stored at -80°C for future use or subjected to further digestion (Accumax; protease / DNAse solution; Innovative Cell Technologies Inc, CA) prior to ImageStream analysis (Amnis, WA). Cells were gated according to spherical shape and yellow fluorescence before automated single-cell image capture.

Biochemical methods

LCMSMS. The Agilent 6400 Series Triple Quadrupole LCMS/MS System was used for this study. Biological compounds optimised for detection included methylarginines (Calbiochem, Nottingham, UK), amino acids; creatinine (all Sigma, Dorset, UK). Biological samples including plasma, urine and tissue lysates were prepared by methanol protein precipitation in a 1:5 dilution, vortexed and the pellet removed by centrifugation. Sample solutions were evaporated to dry in a heat-block and resuspended in mobile phase (0.1%

For Peer Review

formic acid). An internal standard was added (7-deuterated ADMA; Cambridge Isotope Laboratories, MA) before precipitation to allow correction for extraction efficiency and ion suppression at the point of detection (ions in large abundance can out-compete minority ions at the detector). A hypercarb (Thermo Scientific, UK) chromatography column was used and the mobile phase consisted of 0.1% formic acid, 1% acetonitrile (increasing to 50% between 5 and 10 minutes) over a total run time of 15 minutes. Data was collected using Agilent (Berkshire, UK) MassHunter Data Acquisition Software and analysed with MassHunter Qualitative Analysis Software before downloading raw data into MicroSoft Excel for processing. The mass spectrum parameters were as follows: ADMA, mass-to-charge ratio *(m/z)*: 203.3 to 46.0, collision energy (CE): 12; SDMA, *m/z*: 203.3 to 70.2, CE: 24; arginine, *m/z*: 175.2 to 60.1, CE: 8; citrulline, *m/z*: 176.2 to 86.2, CE: 16; glutamine, *m/z*: 147.0 to 56.3, CE: 0; d7-ADMA, *m/z*: 210.0 to 46.0, CE: 24; creatinine *m/z*: 114.0 to 44.0, CE: 12. Standard curves were generated for each substance of interest.

Molecular biological methods

Measurements of routine biochemical variables in patient samples were performed by National Health Service hospital laboratories. NOx (NO2 and NO3) was measured by chemiluminscence with a Sievers Nitric Oxide Analyzer (GE Analytical Instruments, Manchester, UK) as per protocol. Protein concentrations were determined by Bradford assay and Nanodrop.

Tissue genotyping was performed using ReadyMix Taq PCR Reaction Mix (Sigma, Dorset, UK). Tissue mRNA expression was determined by iScript cDNA reverse transcription kit, followed by RT-qPCR (iTaq Fast SYBR Green Supermix with ROX (BioRad, Hertfordshire, UK) using a 7900HT Fast System, Applied Biosystems (Life Technologies, Paisley, UK). All reactions were performed in duplicate and several “housekeeper” sequences were optimised for different types of biological sample with *Pol2a* the most stably expressed gene. Primer sequences are listed in the complete methods.

Proteins were separated and identified using Western Blotting and sodium dodecyl sulfate-polyacrylamide gel electrophoresis (SDS-PAGE) according to standard protocols. A polyclonal goat *DDAH1* antibody was produced by our own group. UMOD antibody was purchased from R & D Systems (MN, USA).

For Peer Review

GAPDH antibody was purchased from Sigma (Dorset, UK) and the Licor Odyssey system (UK) used for protein detection and quantification. Mouse urine UMOD protein was quantified by ELISA according to manufacturers' protocol (Uscn Life Science Inc., PRC).

Histological methods

Frozen sections. Kidneys from the ROSAYFP reporter mouse were fixed overnight in 4% PFA, then 30% sucrose in PBS until full tissue submersion (~4 hours). Specimens were embedded in OCT and snap frozen onto cork discs in methanol cooled on dry ice and stored at -80°C. Sections (5 μM) were cut at -20°C (cryotome CM 1850 Leica Microsystems, Germany) onto poly-L-lysine-coated glass slides. Slides were studied using a Leica SP5 microscope.

Paraffin sections. Harvested organs were fixed in 4% paraformaldehyde (PFA) overnight and then stored in 70% ethanol. Tissues were embedded in paraffin blocks by an automated processor and 5μM sections cut on a microtome and attached to poly-L-lysine-coated glass slides before staining with periodic-acid schiff or picrosirius red (PSR).

Collagen content. Kidney sections were assessed for collagen deposition using a Manual Zeiss Axiophot microscope (Zeiss, NY) through circularly polarized light. Tissue images were obtained with a 2.5X objective lens, recorded on a digital camera (Canon EOS-40D digital SLR; Canon Inc, Tokyo, Japan) and viewed through Canon Utilities EOS software (Canon Inc, Tokyo, Japan). Images were analysed using a Fiji software macro (written by Dr Dirk Dorman, Head of Microscopy, MRC Clinical Sciences Centre, Imperial College, London) to quantify collagen in each whole kidney slice, thus obviating bias. Percentage collagen deposition per total section area (pixels) could then be reported.

Statistical methods. Statistical analysis was performed using the Prism software package (Graph Pad Inc., UK). All data are presented as means ± SEM. For comparisons between two groups for a single variable, a Mann-Whitney U test (non-parametric data or where a normal distribution could not be assumed) was used. Differences between multiple groups were assessed by one-way analysis of variance (ANOVA) followed by Bonferroni's post test for multiple comparisons. Two-way ANOVA was used where comparisons were being made between groups subject to two experimental variables, followed by

For Peer Review

Bonferroni's post test for multiple comparisons. P values of <0.05 were considered statistically significant.

Proteomic analysis (LC-MS/MS)

Urine samples were retrieved from -80°C and thawed in an Eppendorf Thermomixer Comfort mixer at 22ºC, 900 x g for 10 minutes, and then centrifuged at 5ºC, 13000g for 3 minutes. 200µL of sample was mixed 1:5 with 0.1% trifluoroacetic (TFA) acid and subjected to two different solid phase extraction (SPE) steps; reverse-phase SPE (Waters Oasis HLB cartridges, Waters Corporation, MA) and; cation exchange SPE (Waters Oasis MCX cartridges, Waters Corporation, MA). SPE was performed using a manual vacuum manifold (24 port vacuum manifold, Thermo Scientific, DE) & LC-MS grade solvents (Fisher Scientific, UK). Dried samples were solubilised in 40µL of 0.1%TFA, sonicated for 10 minutes and then centrifuged at 5ºC, 13000g for 10 minutes. 10µL of supernatant was transferred to a Bioquote Limited 0.2mL lubricated hydrophobic PCR tube and placed into an autosampler vial ready for LC-MS injection and analysis. A Dionex (Thermo Scientific, DE) Ultimate 3000 nano liquid chromatography system was used to separate peptides prior to mass spectrometric analysis. A volume of 4µL was loaded onto a trap column (Acclaim Pepmap 100, Thermo Scientific, DE) at 8µL/min in 98% water, 2% acetonitrile, 0.1% TFA. Peptides were then eluted on-line to an analytical column (Acclaim Pepmap RSLC, Thermo Scientific, DE) and separated using a ramped gradient with conditions: initial 5 minutes with 4% B (96% A), then 90 minute gradient 4-55% B, then 10 minute isocratic at 100% B, then 5 minute isocratic at 4% B (solvent A: 98% water, 2% acetonitrile, 0.1% formic acid; solvent B: 20% water, 80% acetonitrile, 0.1% formic acid). Eluted peptides were analysed using LTQ XL Orbitrap (Thermo Scientific, DE) operating in positive polarity, top 4 CID (collision-induced dissociation) method. Ions for dissociation were determined from initial 15000 resolution MS scan (event 1) followed by CID on the top 4 most abundant ions. CID conditions: default charge state 2, 2.0 m/z isolation width, normalised collision energy 35.0, Activation Q value 0.25, activation time 30ms, lock mass value of 445.120030 m/z used.

Proteomic data analysis. Raw files were searched against UniprotKB/Swiss-Prot database (version 10032012) restricted to mouse entries using Mascot

For Peer Review

v2.3.01. Relative quantification of peptides was performed by extracted ion chromatograms of parent ions using an in-house developed software.

Human cohort data methods

Participants. Appropriate research ethics committee, NHS management, and institutional review board approvals were in place for both cohort studies. Studies were conducted in accordance with the Declaration of Helsinki Principles and written informed consent was obtained from all subjects.

The London Protocol Biopsy Study consisted of patients undergoing protocol biopsy following first kidney alone transplant as per routine clinical care. Subjects were recruited from the Royal Free Hospital NHS Trust transplant clinic. The Virginia cohort underwent similar protocol biopsies but two patients with kidney after liver transplant were also included. Follow-up biochemistry was performed in local laboratories as per routine clinical care and eGFR results obtained with a minimum interval of 1 week between data-points in the London study and monthly in the Virginia study.

Biopsy Tissue RT-qPCR. Protocol biopsy samples were preserved in '*RNA Later'* (Qiagen, UK) at the bedside, before being stored at -70°C. Tissue was lysed in a 1% β-mercaptoethanol (β-ME) containing proprietary lysis buffer (RLT, Qiagen, UK). RNA was extracted using a column system (RNeasy kit, Qiagen, UK) according to the manufacturer's instructions. No carrier RNA was used. Resulting RNA samples were examined using a *'Nanodrop'* spectrophotometer (Thermo Scientific, DE) prior to reverse transcription. First strand cDNA was synthesized using qScript cDNA Synthesis Kit (Quanta Biosciences, MD).

In the London cohort primers were designed to amplify cDNA from human DDAH1. Primer sequences for human control genes were either publically available, or listed elsewhere. [21] Absolute quantification of cDNA was performed on a 7900HT Real-Time PCR System (Applied Biosystems, Life Technologies, UK). RT-qPCR results from the genes of interest were normalised to the 3 most stable of 6 control genes *ACTβ*, β-2 microglobulin *(β2M*), hypoxanthine phosphoribosyltransferase 1 (*HPRT*), ribosomal protein 13A (*RPL13A*), succinate deghydrogenase complex subunit A flavoprotein (*SDHA*) and TATA box binding protein (*TBP*). In the Virginia cohort a taqman

For Peer Review

primer approach was used. Expression of *DDAH1* and *AGXT2* were performed and corrected to a single reference gene (beta-2 microglobulin). In both cohorts genes of interest were normalized to vary between zero and one. Ten samples were quantified at both sites demonstrating high levels of inter-centre agreement.

Uromodulin in the human cohort was measured using ELISA (MD Bioproducts, Zurich) as per manufacturer's instructions.

Human cohort data statistical methods. A multilevel multivariable approach was used to model eGFR over time in each of the two cohorts. Follow-up was commenced at the time of protocol biopsy and MDRD GFR measurements out to 1-year following biopsy examined. eGFR values were nested within patients using both a random-intercept and random-slope and the slope of eGFR quantified by the inclusion time variable. The impact of gene expression on eGFR decline was quantified by the addition of an expression x time interaction. Residuals were examined to ensure there was no substantial deviation from normality.

Acknowledgements

This work was funded by the Medical Research Council (JL), Imperial College London Biomedical Research Centre (JT), Chain-Florey Clinical Research Fellowship, MRC (JT) and the British Heart Foundation (JL). PG 002/05. Some of the data presented here has been previously been presented in abstract form for poster presentation (ASN Kidney Week 2013). Work in CSW's laboratory is supported by grants from the NIH (DK-49870 and HL-68686).

Statement of competing financial interests

None.

For Peer Review

References

1 Jha, V., Wang, A. Y. & Wang, H. The impact of CKD identification in large countries: the burden of illness. *Nephrology, dialysis, transplantation : official publication of the European Dialysis and Transplant Association - European Renal Association* **27 Suppl 3**, iii32-38,(2012).

2 Alwan, A. W. H. O. Global status report on noncommunicable diseases 2010. 176 (2011).

3 Baylis, C. Nitric oxide synthase derangements and hypertension in kidney disease. *Curr. Opin. Nephrol. Hypertens.* **21**, 1-6,(2012).

4 Moncada, S., Palmer, R. M. & Higgs, E. A. Nitric oxide: physiology, pathophysiology, and pharmacology. *Pharmacol. Rev.* **43**, 109-142,(1991).

5 Caplin, B., Wang, Z., Slaviero, A., Tomlinson, J., Dowsett, L., Delahaye, M., Salama, A., Wheeler, D. C. & Leiper, J. Alanine-glyoxylate aminotransferase-2 metabolizes endogenous methylarginines, regulates NO, and controls blood pressure. *Arterioscler. Thromb. Va c. Biol.* **32**, 2892-2900,(2012).

6 Caplin, B. & Leiper, J. Endogenous nitric oxide synthase inhibitors in the biology of disease: markers, mediators, and regulators? *Arterioscler. Thromb. Va c. Biol.* **32**, 1343-1353,(2012).

7 Onozato, M. L., Tojo, A., Leiper, J., Fujita, T., Palm, F. & Wilcox, C. S. Expression of NG,NG-dimethylarginine dimethylaminohydrolase and protein arginine N-methyltransferase isoforms in diabetic rat kidney: effects of angiotensin II receptor blockers. *Diabetes* **57**, 172-180,(2008).

8 Mount, P. F. & Power, D. A. Nitric oxide in the kidney: functions and regulation of synthesis. *Acta physiologica* **187**, 433-446,(2006).

9 Majid, D. S. & Navar, L. G. Nitric oxide in the control of renal hemodynamics and excretory function. *Am. J. Hypertens.* **14**, 74S-82S,(2001).

10 Carlstrom, M., Lai, E. Y., Ma, Z., Steege, A., Patzak, A., Eriksson, U. J., Lundberg, J. O., Wilcox, C. S. & Persson, A. E. Superoxide dismutase 1 limits renal microvascular remodeling and attenuates arteriole and blood pressure responses to angiotensin II via modulation of nitric oxide bioavailability. *Hypertension* **56**, 907-913,(2010).

11 Wilcox, C. S. Role of macula densa NOS in tubuloglomerular feedback. *Curr. Opin. Nephrol. Hypertens.* **7**, 443-449,(1998).

12 Ortiz, P. A. & Garvin, J. L. Role of nitric oxide in the regulation of nephron transport. *Am J Physiol Renal Physiol* **282**, F777-784,(2002).

13 Tojo, A., Welch, W. J., Bremer, V., Kimoto, M., Kimura, K., Omata, M., Ogawa, T., Vallance, P. & Wilcox, C. S. Colocalization of demethylating enzymes and NOS and functional effects of methylarginines in rat kidney. *Kidney Int.* **52**, 1593-1601,(1997).

14 Nijveldt, R. J., Van Leeuwen, P. A., Van Guldener, C., Stehouwer, C. D., Rauwerda, J. A. & Teerlink, T. Net renal extraction of asymmetrical (ADMA) and symmetrical (SDMA) dimethylarginine in fasting humans. *Nephrology, dialysis, transplantation : official publication of the*

For Peer Review

European Dialysis and Transplant Association - European Renal Association **17**, 1999-2002,(2002).

15 Vallance, P., Leone, A., Calver, A., Collier, J. & Moncada, S. Accumulation of an endogenous inhibitor of nitric oxide synthesis in chronic renal failure. *Lancet* **339**, 572-575,(1992).

16 Boger, R. H., Sullivan, L. M., Schwedhelm, E., Wang, T. J., Maas, R., Benjamin, E. J., Schulze, F., Xanthakis, V., Benndorf, R. A. & Vasan, R. S. Plasma asymmetric dimethylarginine and incidence of cardiovascular disease and death in the community. *Circulation* **119**, 1592-1600,(2009).

17 Schulze, F., Lenzen, H., Hanefeld, C., Bartling, A., Osterziel, K. J., Goudeva, L., Schmidt-Lucke, C., Kusus, M., Maas, R., Schwedhelm, E., Strodter, D., Simon, B. C., Mugge, A., Daniel, W. G., Tillmanns, H., Maisch, B., Streichert, T. & Boger, R. H. Asymmetric dimethylarginine is an independent risk factor for coronary heart disease: results from the multicenter Coronary Artery Risk Determination investigating the Influence of ADMA Concentration (CARDIAC) study. *Am. Heart J.* **152**, 493 e491-498,(2006).

18 Zoccali, C., Bode-Boger, S., Mallamaci, F., Benedetto, F., Tripepi, G., Malatino, L., Cataliotti, A., Bellanuova, I., Fermo, I., Frolich, J. & Boger, R. Plasma concentration of asymmetrical dimethylarginine and mortality in patients with end-stage renal disease: a prospective study. *Lancet* **358**, 2113-2117,(2001).

19 Young, J. M., Terrin, N., Wang, X., Greene, T., Beck, G. J., Kusek, J. W., Collins, A. J., Sarnak, M. J. & Menon, V. Asymmetric dimethylarginine and mortality in stages 3 to 4 chronic kidney disease. *Clinical journal of the American Society of Nephrology : CJASN* **4**, 1115-1120,(2009).

20 Fliser, D., Kronenberg, F., Kielstein, J. T., Morath, C., Bode-Boger, S. M., Haller, H. & Ritz, E. Asymmetric dimethylarginine and progression of chronic kidney disease: the mild to moderate kidney disease study. *Journal of American Society Nephrology* **16**, 2456-2461,(2005).

21 Caplin, B., Nitsch, D., Gill, H., Hoefield, R., Blackwell, S., MacKenzie, D., Cooper, J. A., Middleton, R. J., Talmud, P. J., Veitch, P., Norman, J., Wheeler, D. C. & Leiper, J. M. Circulating methylarginine levels and the decline in renal function in patients with chronic kidney disease are modulated by DDAH1 polymorphisms. *Kidney Int.* **77**, 459-467,(2010).

22 Li, H., Zhou, X., Davis, D. R., Xu, D. & Sigmund, C. D. An androgen-inducible proximal tubule-specific Cre recombinase transgenic model. *Am J Physiol Renal Physiol* **294**, F1481-1486,(2008).

23 Leiper, J., Nandi, M., Torondel, B., Murray-Rust, J., Malaki, M., O'Hara, B., Rossiter, S., Anthony, S., Madhani, M., Selwood, D., Smith, C., Wojciak-Stothard, B., Rudiger, A., Stidwill, R., McDonald, N. Q. & Vallance, P. Disruption of methylarginine metabolism impairs vascular homeostasis. *Nat. Med.* **13**, 198-203,(2007).

24 Muller, V., Tain, Y. L., Croker, B. & Baylis, C. Chronic nitric oxide deficiency and progression of kidney disease after renal mass reduction in the C57Bl6 mouse. *Am. J. Nephrol.* **32**, 575-580,(2010).

25 Arcos, M. I., Fujihara, C. K., Sesso, A., de Almeida Prado, E. B., de Almeida Prado, M. J., de Nucci, G. & Zatz, R. Mechanisms of

albuminuria in the chronic nitric oxide inhibition model. *Am J Physiol Renal Physiol* **279**, F1060-1066,(2000).

26 Suda, O., Tsutsui, M., Morishita, T., Tanimoto, A., Horiuchi, M., Tasaki, H., Huang, P. L., Sasaguri, Y., Yanagihara, N. & Nakashima, Y. Long-term treatment with N(omega)-nitro-L-arginine methyl ester causes arteriosclerotic coronary lesions in endothelial nitric oxide synthase-deficient mice. *Circulation* **106**, 1729-1735,(2002).

27 Ravani, P., Tripepi, G., Malberti, F., Testa, S., Mallamaci, F. & Zoccali, C. Asymmetrical dimethylarginine predicts progression to dialysis and death in patients with chronic kidney disease: a competing risks modeling approach. *J. Am. Soc. Nephrol.* **16**, 2449-2455,(2005).

28 Mihout, F., Shweke, N., Bige, N., Jouanneau, C., Dussaule, J. C., Ronco, P., Chatziantoniou, C. & Boffa, J. J. Asymmetric dimethylarginine (ADMA) induces chronic kidney disease through a mechanism involving collagen and TGF-beta1 synthesis. *The Journal of pathology* **223**, 37-45,(2011).

29 Matsumoto, Y., Ueda, S, Yamagishi, S, Matsuguma, K, Shibata, R, Fukami, K, Matsuoka, H, Imaizumi, T, and Okuda, S. Dimethylarginine dimethylaminohydrolase prevents progression of renal dysfunction by inhibiting loss of peritubular capillaries and tubulointerstitial fibrosis in a rat model of chronic kidney disease. *J Am Soc Nephrol* **18**, 1525-1533,(2007).

30 Jacobi, J., Maas, R, Cordasic, N, Koch, K, Schmieder, RE, Boger, RH, and Hilgers, KF. (2008), "Role of asymmetric dimethylarginine for angiotensin II-induced target organ damage in mice". Am J Physiol Heart Circ Physiol 294, H1058-H1066 Role of asymmetric dimethylarginine for angiotensin II-induced target organ damage in mice. *Am J Physio Heart Circ Physiol* **294**, H1058-H1066,(2008).

31 Xia, W., Szomor, Z., Wang, Y. & Murrell, G. A. Nitric oxide enhances collagen synthesis in cultured human tendon cells. *Journal of orthopaedic research : official publication of the Orthopaedic Research Society* **24**, 159-172,(2006).

32 Thornton, F. J., Schaffer, M. R., Witte, M. B., Moldawer, L. L., MacKay, S. L., Abouhamze, A., Tannahill, C. L. & Barbul, A. Enhanced collagen accumulation following direct transfection of the inducible nitric oxide synthase gene in cutaneous wounds. *Biochem. Biophys. Res. Commun.* **246**, 654-659,(1998).

33 Shi, H. P., Efron, D. T., Most, D., Tantry, U. S. & Barbul, A. Supplemental dietary arginine enhances wound healing in normal but not inducible nitric oxide synthase knockout mice. *Surgery* **128**, 374-378,(2000).

34 Guix, F. X., Uribesalgo, I., Coma, M. & Munoz, F. J. The physiology and pathophysiology of nitric oxide in the brain. *Prog. Neurobiol.* **76**, 126-152,(2005).

35 Chatziantoniou, C., Boffa, J. J., Ardaillou, R. & Dussaule, J. C. Nitric oxide inhibition induces early activation of type I collagen gene in renal resistance vessels and glomeruli in transgenic mice. Role of endothelin. *The Journal of clinical investigation* **101**, 2780-2789,(1998).

For Peer Review

36 Peters, H., Border, W. A. & Noble, N. A. L-Arginine supplementation increases mesangial cell injury and subsequent tissue fibrosis in experimental glomerulonephritis. *Kidney Int.* **55**, 2264-2273,(1999).

37 Eberhardt, W. & Pfeilschifter, J. Nitric oxide and vascular remodeling: spotlight on the kidney. *Kidney Int. Suppl.*, S9-S16,(2007).

38 Peters, H., Border, W. A., Ruckert, M., Kramer, S., Neumayer, H. H. & Noble, N. A. L-arginine supplementation accelerates renal fibrosis and shortens life span in experimental lupus nephritis. *Kidney Int.* **63**, 1382-1392,(2003).

39 Weinberg, J. B., Granger, D. L., Pisetsky, D. S., Seldin, M. F., Misukonis, M. A., Mason, S. N., Pippen, A. M., Ruiz, P., Wood, E. R. & Gilkeson, G. S. The role of nitric oxide in the pathogenesis of spontaneous murine autoimmune disease: increased nitric oxide production and nitric oxide synthase expression in MRL-lpr/lpr mice, and reduction of spontaneous glomerulonephritis and arthritis by orally administered NG-monomethyl-L-arginine. *The Journal of experimental medicine* **179**, 651-660,(1994).

40 Pullamsetti, S. S., Savai, R., Dumitrascu, R., Dahal, B. K., Wilhelm, J., Konigshoff, M., Zakrzewicz, D., Ghofrani, H. A., Weissmann, N., Eickelberg, O., Guenther, A., Leiper, J., Seeger, W., Grimminger, F. & Schermuly, R. T. The role of dimethylarginine dimethylaminohydrolase in idiopathic pulmonary fibrosis. *Sci Transl Med* **3**, 87ra53.

41 Bachmann, S., Metzger, R. & Bunnemann, B. Tamm-Horsfall protein-mRNA synthesis is localized to the thick ascending limb of Henle's loop in rat kidney. *Histochemistry* **94**, 517-523,(1990).

42 Drenning, J. A., Lira, V. A., Simmons, C. G., Soltow, Q. A., Sellman, J. E. & Criswell, D. S. Nitric oxide facilitates NFAT-dependent transcription in mouse myotubes. *Am J Physiol Cell Physiol* **294**, C1088-1095,(2008).

43 Liu, X. K., Abernethy, D. R. & Andrawis, N. S. Nitric oxide inhibits Oct-1 DNA binding activity in cultured vascular smooth muscle cells. *Life Sci.* **62**, 739-749,(1998).

44 Kim, H. T., Song, I. Y. & Piedrahita, J. Kidney-specific activity of the bovine uromodulin promoter. *Transgenic Res.* **12**, 191-201,(2003).

45 Rampoldi, L., Scolari, F., Amoroso, A., Ghiggeri, G. & Devuyst, O. The rediscovery of uromodulin (Tamm-Horsfall protein): from tubulointerstitial nephropathy to chronic kidney disease. *Kidney Int.* **80**, 338-347,(2011).

46 Trudu, M., Janas, S., Lanzani, C., Debaix, H., Schaeffer, C., Ikehata, M., Citterio, L., Demaretz, S., Trevisani, F., Ristagno, G., Glaudemans, B., Laghmani, K., Dell'antonio, G., Bochud, M., Burnier, M., Devuyst, O., Martin, P. Y., Mohaupt, M., Paccaud, F., Pechere-Bertschi, A., Vogt, B., Ackermann, D., Ehret, G., Guessous, I., Ponte, B., Pruijm, M., Loffing, J., Rastaldi, M. P., Manunta, P. & Rampoldi, L. Common noncoding UMOD gene variants induce salt-sensitive hypertension and kidney damage by increasing uromodulin expression. *Nat. Med.*,(2013).

47 Heffner, C. S., Herbert Pratt, C., Babiuk, R. P., Sharma, Y., Rockwood, S. F., Donahue, L. R., Eppig, J. T. & Murray, S. A. Supporting

For Peer Review

conditional mouse mutagenesis with a comprehensive cre characterization resource. *Nature communications* **3**, 1218,(2012).

48 Buerger, A., Rozhitskaya, O., Sherwood, M. C., Dorfman, A. L., Bisping, E., Abel, E. D., Pu, W. T., Izumo, S. & Jay, P. Y. Dilated cardiomyopathy resulting from high-level myocardial expression of Cre-recombinase. *J. Card. Fail.* **12**, 392-398,(2006).

49 Forni, P. E., Scuoppo, C., Imayoshi, I., Taulli, R., Dastru, W., Sala, V., Betz, U. A., Muzzi, P., Martinuzzi, D., Vercelli, A. E., Kageyama, R. & Ponzetto, C. High levels of Cre expression in neuronal progenitors cause defects in brain development leading to microencephaly and hydrocephaly. *The Journal of neuroscience : the official journal of the Society for Neuroscience* **26**, 9593-9602,(2006).

50 Naiche, L. A. & Papaioannou, V. E. Cre activity causes widespread apoptosis and lethal anemia during embryonic development. *Genesis* **45**, 768-775,(2007).

51 Norden, A. G., Sharratt, P., Cutillas, P. R., Cramer, R., Gardner, S. C. & Unwin, R. J. Quantitative amino acid and proteomic analysis: very low excretion of polypeptides >750 Da in normal urine. *Kidney Int.* **66**, 1994-2003,(2004).

For Peer Review

		London		Virginia	
Sex, n (%)	female	19	(51.35)	14	(38.9)
Age, median (IQR)		47	(40 to 58)	55	(44.5 to 61)
Ethnicity, n (%)	south asian	4	(10.81)	0	(0)
	black	13	(35.14)	7	(19.4)
	other	3	(8.11)	1	(2.8)
	white	17	(45.95)	28	(77.8)
Donor type, n (%)	live	9	(24.32)	1	(2.8)
Donor age, median (IQR)		53	(48 to 61)	47	(23 to 53)
DGF, n (%)		21	(56.75)	14	(38.9)
Rejection prior to protocol biopsy, n (%)		0	(0)	1	(2.8)
eGFR at biopsy, mean (SD)		52.9	(17.7)	56.2	(19)
UMOD, median (IQR)		8.1	(2.7 to 15.2)		

Table 1. Demographics of two human renal transplant cohorts.
DGF, delayed graft function. eGFR, estimated glomerular filtration rate. UMOD, uromodulin.

For Peer Review

	London		Virginia	
	Estimate	95% CI	Estimate	95% CI
GFR change over time mL/min/1.72m2 per day	0.032	0.014 to 0.049	-0.01	-0.025 to 0.005
Increase in GFR at biopsy mL/min/1.72m2 per unit MAME	16.2	-7.3 to 43.4	**32.7**	**13.4 to 52.0**
Change in GFR over time per mL/min/1.72m2 per unit MAME per day	**-0.065**	**-0.107 to -0.023**	**-0.050**	**-0.098 to -0.001**

Table 2. Standard deviation of eGFR estimates: (i) between subject at baseline (intercept): London, 16.2ml/min per 1.73m^2 (95% CI, 12.8-20.6); Virginia, 14.9ml/min per 1.73m^2 (95% CI, 11.4-19.5); (ii) between subject over time (slope): London, 0.02ml/ min per 1.73m^2 per day (95% CI, 0.01–0.03); Virginia, 0.03ml/min per 1.73m^2 per day (95% CI, 0.02-0.05); (iii) within subject: London, 7.1ml/min per 1.73m^2 (95% CI, 6.6–7.5); Virginia, 7.3ml/min per 1.73m^2 (95% CI, 6.8-7.9). Correlation between baseline eGFR (intercept) and slope: London: 0.06 (95% CI, -0.49-0.57); Virginia: 0.17 (95% CI, -0.25-0.54). A decline of 0.05-0.065 mL/min/1.72m^2/day per unit MAME may appear trivial, but a 50% higher renal MAME expression would be reflected in an additional annual rate of renal function decline of 9-12.0 mL/min/1.72m^2 (MAME expression units across these cohorts were normalized to values between 0 and 1).

For Peer Review

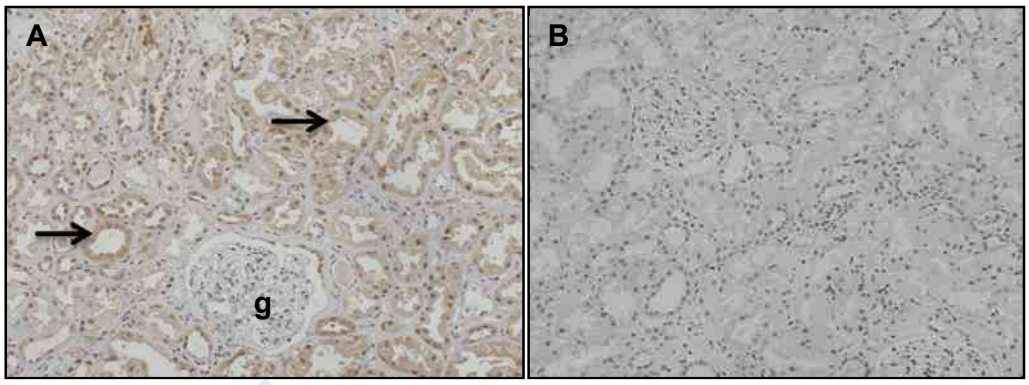

Figure 1. Immunohistochemical staining for *DDAH1*. Human allograft protocol biopsy tissue. **A**, *DDAH1* staining is seen in the epithelial cells of the proximal tubule (arrows) and not in the glomerulus (**g**) or control (**B**; *DDAH1* antibody pre-incubated with *DDAH1* peptide).

For Peer Review

Figure 2. Generation of the *ROSAYFP* reporter mouse (A-C) and *Ddah1*$^{PT-/-}$ mouse strains (D-H).
A, Schematic of conditional *YFP* expression in the reporter mouse. **B,** ImageStream flow cytometry reveals *YFP* expression in renal tubular cells isolated from the *KAPiCre*+ genotype but not *KAPiCre*-. R2 gating for sphericity, R4 gating for fluorescence. Brightfield and yellow fluorescent single cell images are displayed (**B**, *KAPiCre*+). **C**, *YFP* fluorescence visible in unstained kidney sections from *KAPiCre*+ mice and not *KAPiCre*-. Representative of n=3. Bars = 50 µm.
D, Schematic of conditional *Ddah1* deletion in the *Ddah1*$^{PT-/-}$ mouse. **E,** Kidney tissue end-point PCR genotyping for *KAPiCre* (KC), floxed *Ddah1* and deleted *Ddah1* sequences reveals gene excision in *KAPiCre* + (*Ddah1*$^{PT-/-}$) but not *KAPiCre*– (*Ddah1*$^{fl/fl}$) genotypes (2 per genotype shown for representation). Excision is detected within liver and brain, however quantitative RT-qPCR analysis reveals significant *Ddah1* mRNA reduction within kidney but not other organs (**F**). **G**, Kidney tissue DDAH1 protein (4 for representation in Western blot) and **H**, enzymatic activity are significantly reduced (70-80%). Mann-Whitney U test, n=6 (*Ddah1*$^{fl/fl}$) and n=8 (*Ddah1*$^{PT-/-}$), *p<0.05 ***<0.001.

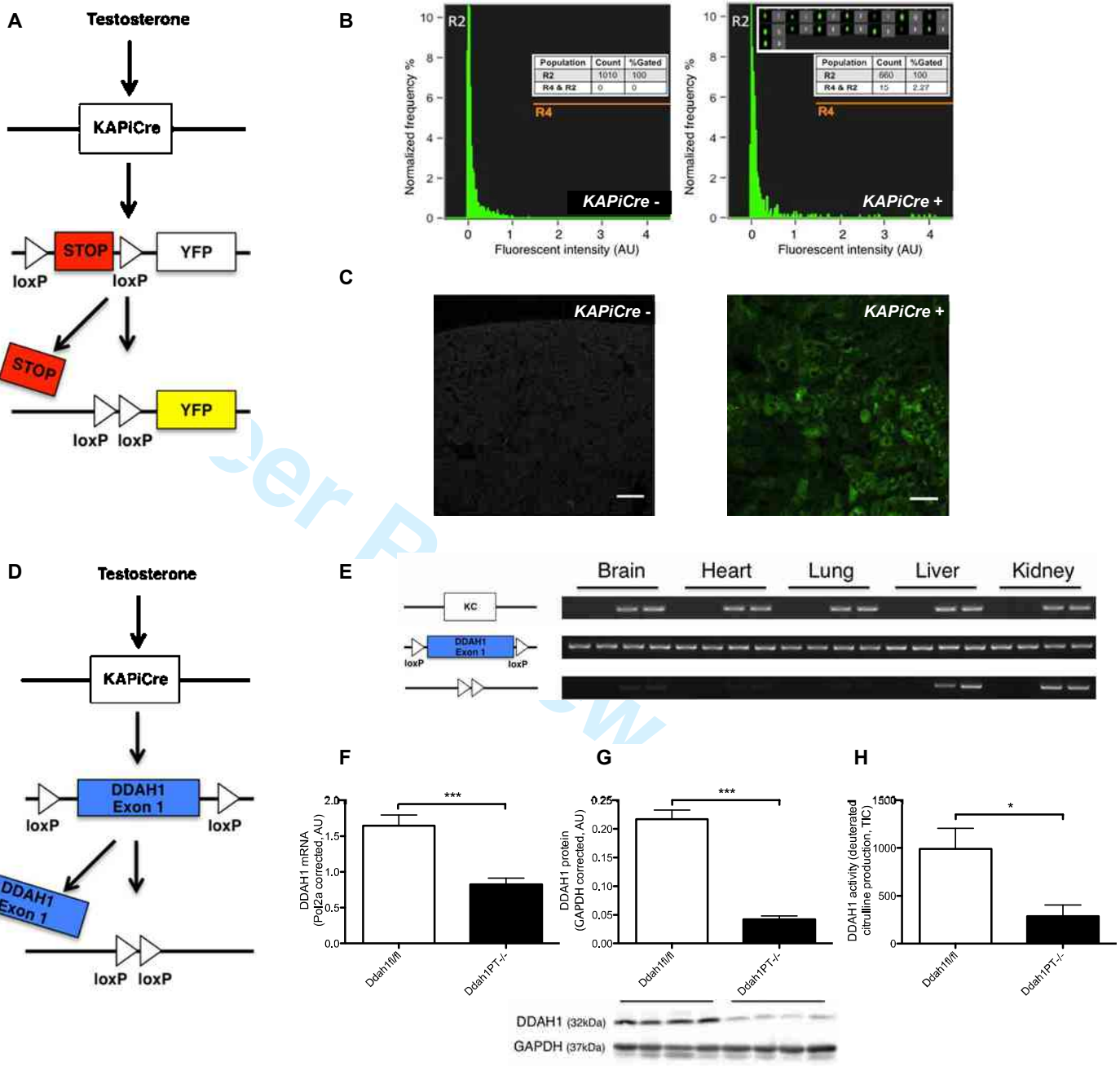

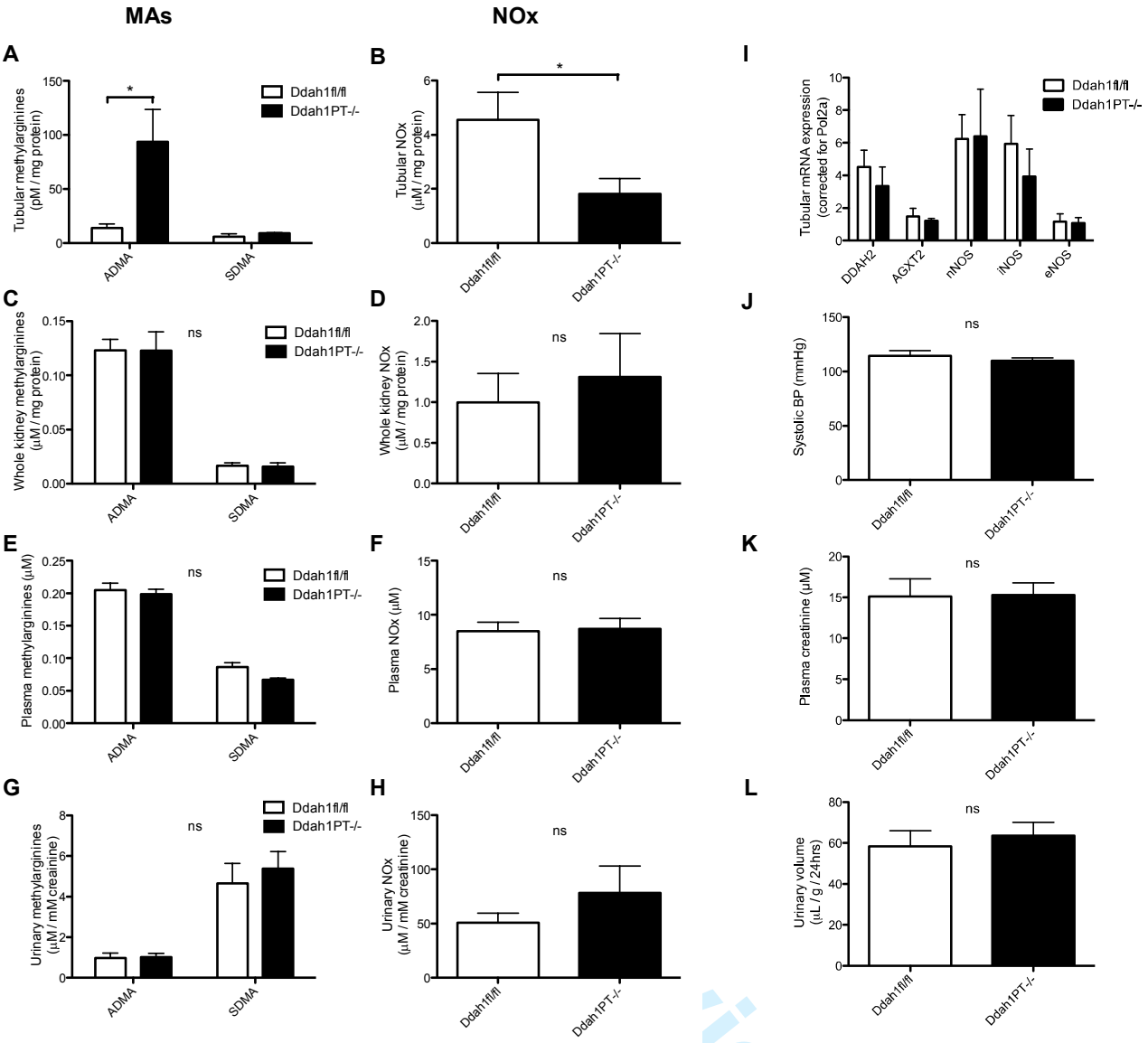

Figure 3. Effects of PT-specific *Ddah1* deletion upon ADMA and NO are tubule-specific. **A** and **B**, tubular cells isolated from *Ddah1*$^{PT-/-}$ mice contained significantly higher ADMA and lower NO concentrations. SDMA, a methylarginine not a substrate for *DDAH1*, was unaffected. **C-H,** these changes were not evident in whole kidney tissue, plasma or urine. **I,** Tubular cell expression of other MAMEs and NOS isoforms (neuronal, inducible and endothelial), was unaffected in *Ddah1*$^{PT-/-}$ mice. Similarly, systolic BP, plasma creatinine and urinary volumes were not altered (**J-L**). Mann-Whitney U test, n=6 each group, *p<0.05. (NOTE: The measurement of urinary NOx is not necessarily an accurate determination of renal NOS activity, particularly in the context of a nitrate-containing diet).

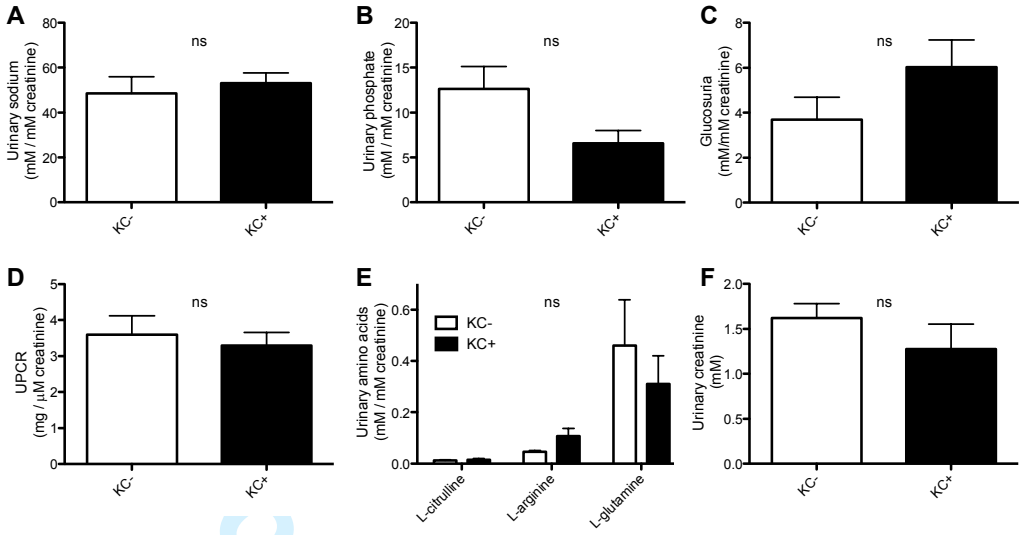

Figure 4. Effects of PT-specific *Ddah1* deletion upon urinary electrolytes, protein and amino acids at baseline. No consistent changes in urine biochemistry were identified in *Ddah1*$^{PT-/-}$ mice. Amino acids L-citrulline and L-arginine being product and substrate for NO synthesis respectively; L-glutamine was selected due to abundance in urine and has been shown to be elevated in patients with tubular dysfunction (Fanconi's syndrome). [51] All values corrected for creatinine concentration. Mann-Whitney U test. n=8 (*Ddah1*$^{fl/fl}$) and n=20 (*Ddah1*$^{PT-/-}$).

For Peer Review

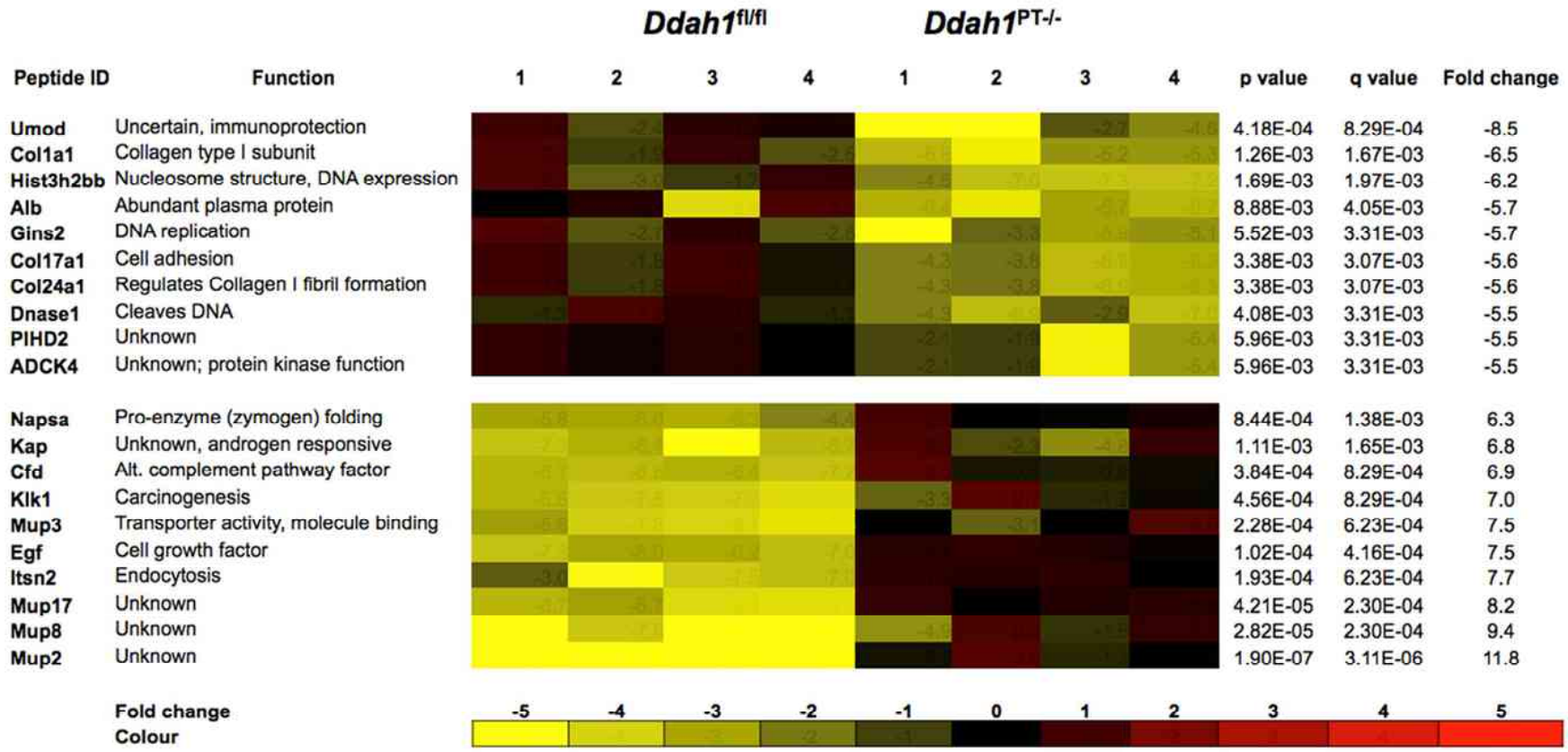

Figure 5. Heat map of urinary proteomic analysis following PT-specific *Ddah1* deletion at baseline. 82 of 1057 peptides screened were significantly altered by *Ddah1* deletion. The ten most significantly down- and upregulated peptides are represented here. (q values represent values of significance adjusted for multiple comparisons, n=4).

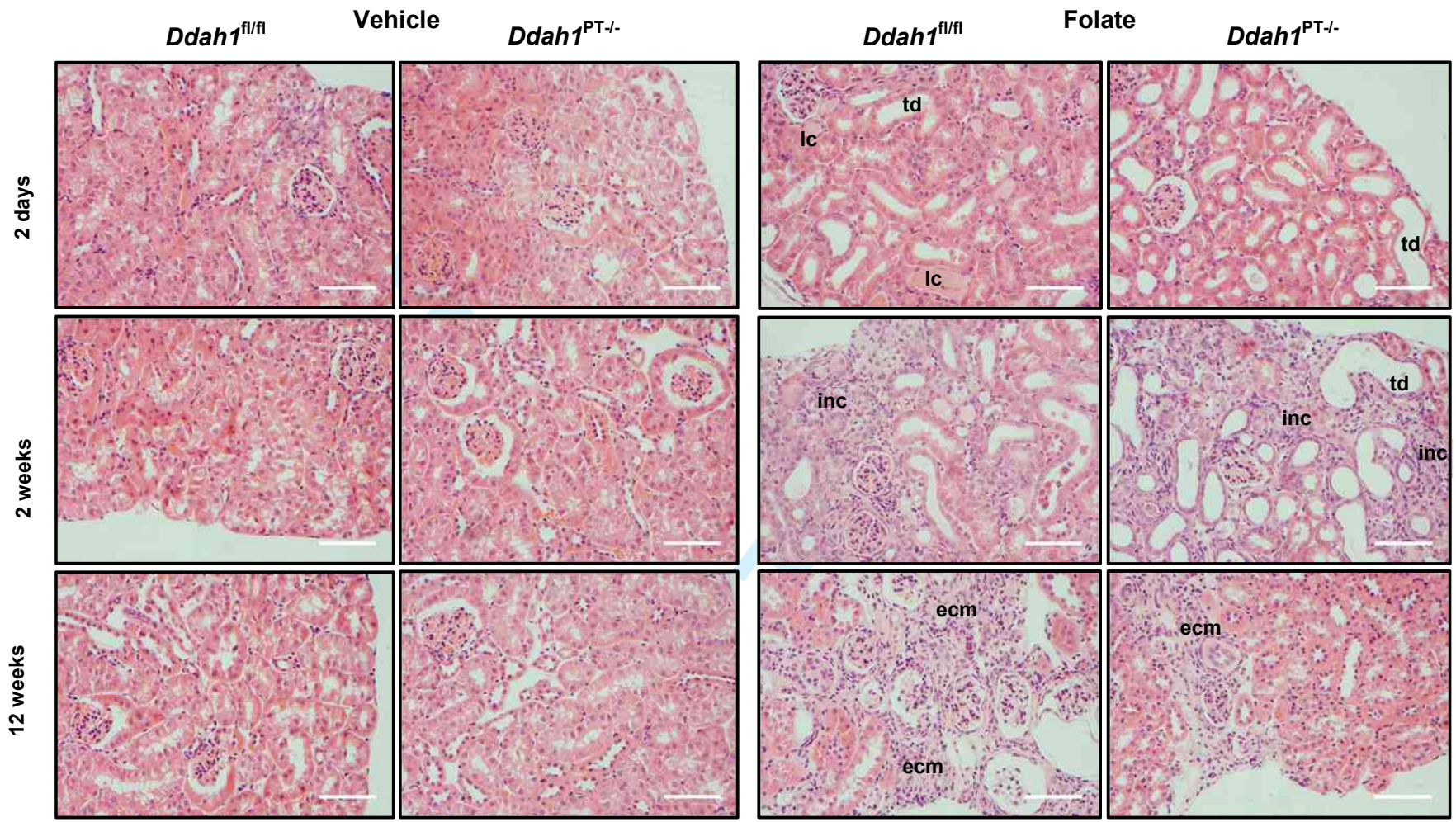

Figure 6. Histological appearances of folate nephropathy in *Ddah1*$^{PT-/-}$ mice and controls. At 2 days and 2 weeks following a single IP folate injection, significant disease was evident including; tubular dilatation (**td**) and epithelial cell flattening; luminal casts (**lc**) and more significantly at 2 weeks; tubulointerstitial inflammatory cell infiltrates (**inc**). At 12 weeks following folate injury, tubulointerstitial fibrosis / extra-cellular matrix (**ecm**) deposition was evident. There were no gross histological differences between *Ddah1*$^{fl/fl}$ and *Ddah1*$^{PT-/-}$ mice however, analysis of collagen deposition and pro-fibrotic cytokine gene expression revealed protection from PT-specific Ddah1 deletion (Figure 7). Images representative of n=9 (*Ddah1*$^{fl/fl}$), n=12 (*Ddah1*$^{PT-/-}$). Bars = 50 μm.

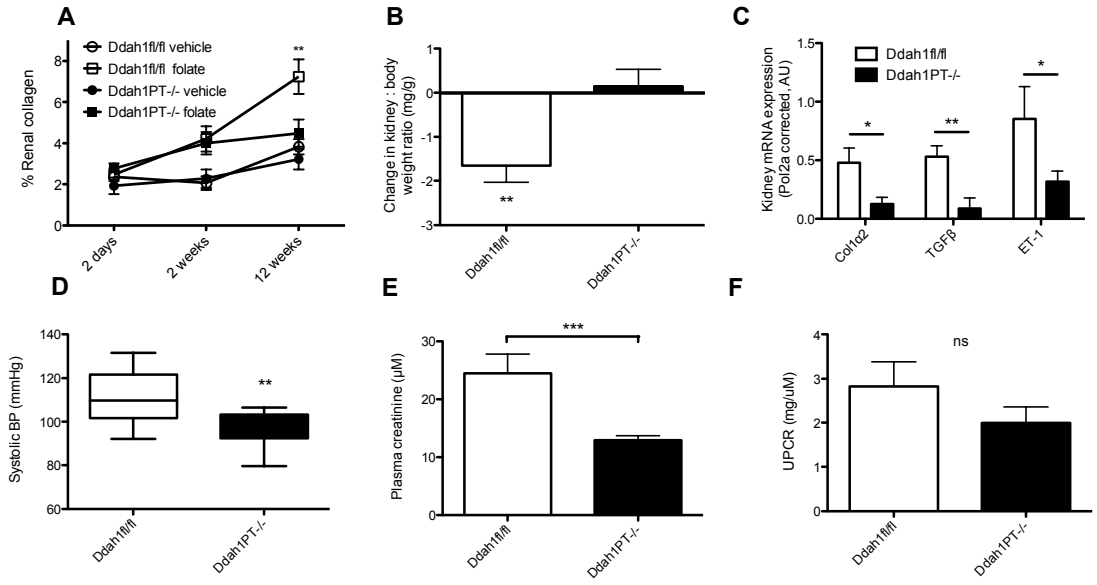

Figure 7. Effects of PT-specific DDAH1 deletion at 12 weeks following folate. A, Renal collagen deposition was significantly reduced in *Ddah1*$^{PT-/-}$ mice versus *Ddah1*$^{fl/fl}$ controls (4.5 vs 7.2%; p<0.05). Two-way ANOVA with Bonferroni's post test, *p<0.05. **B,** *Ddah1*$^{PT-/-}$ mice had significantly attenuated kidney:body weight ratio reduction compared to *Ddah1*$^{fl/fl}$ controls (p<0.001; values are deviations from means of vehicle-treated controls). **C,** RT-qPCR analysis revealed significantly lower renal tissue pro-fibrotic cytokine expression in *Ddah1*$^{PT-/-}$ mice. Collagen 1 subunit α2 (*Col1α2*) >3-fold (p<0.05); transforming growth factor β (*TGFβ*) >5-fold (p<0.01); and endothelin-1 (*ET-1*) almost 3-fold (p<0.05). **D** and **E,** systolic BP and serum creatinine were lower in *Ddah1*$^{PT-/-}$ mice (**p<0.01 and ***p<0.001 respectively). **F,** proteinuria according to urine protein:creatinine ratio (UPCR) was reduced in *Ddah1*$^{PT-/-}$ mice but not statistically significant. Mann-Whitney U test unless otherwise stated, n=9 (*Ddah1*$^{fl/fl}$) and n=12 (*Ddah1*$^{PT-/-}$). *p<0.05, **p<0.01, ***p<0.001.

For Review

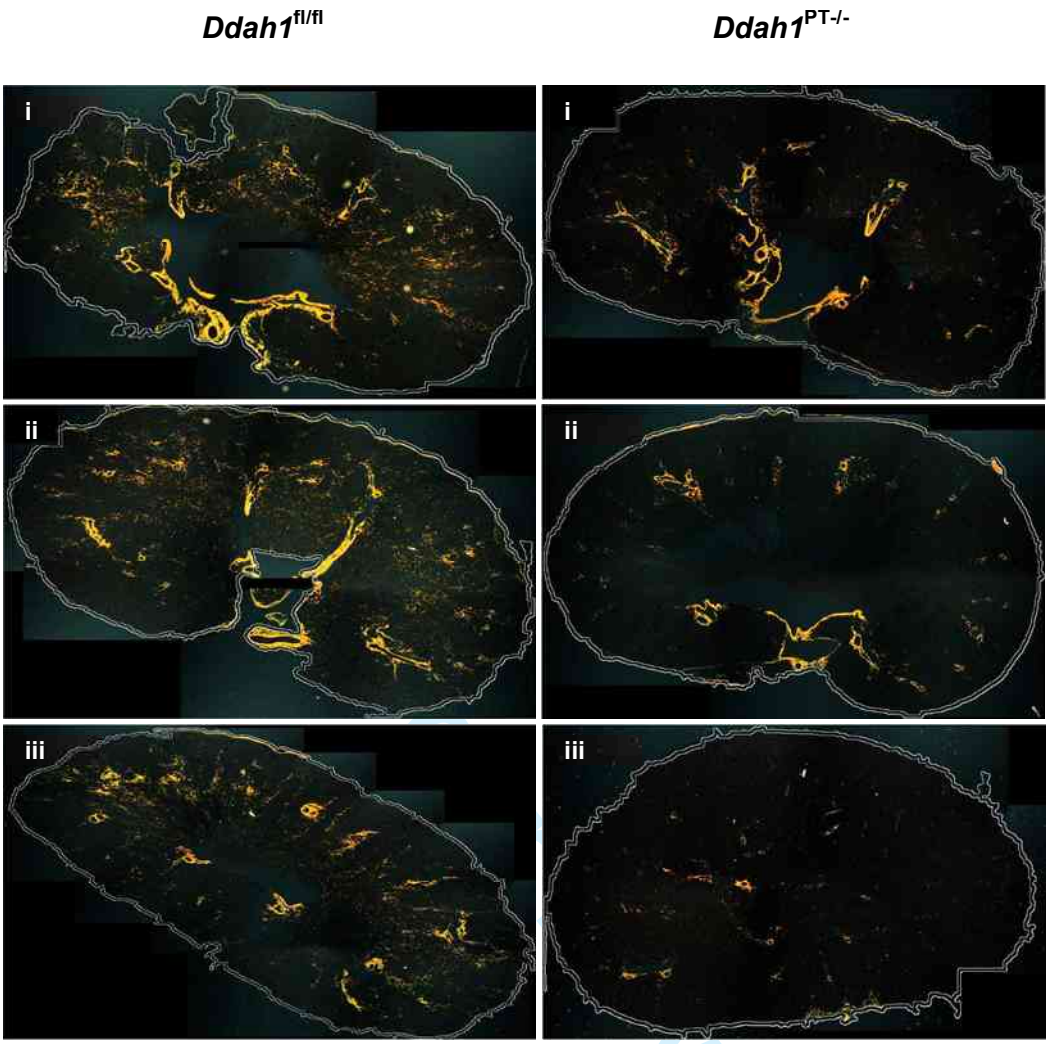

Figure 8. Reduced renal collagen deposition in PT-specific DDAH1 deleted mice at 12 weeks following folate. Kidney sections stained with picrosirius red and viewed through circularly polarised light. Images taken at x25 magnification were processed using Image J software. Images were stitched to produce a complete kidney section image, total section area defined by texture thresholding and collagen (yellow) was quantified as a percentage of total kidney section area. n=3 shown here representative of n=9 (*Ddah1*$^{fl/fl}$) and n=12 (*Ddah1*$^{PT-/-}$).

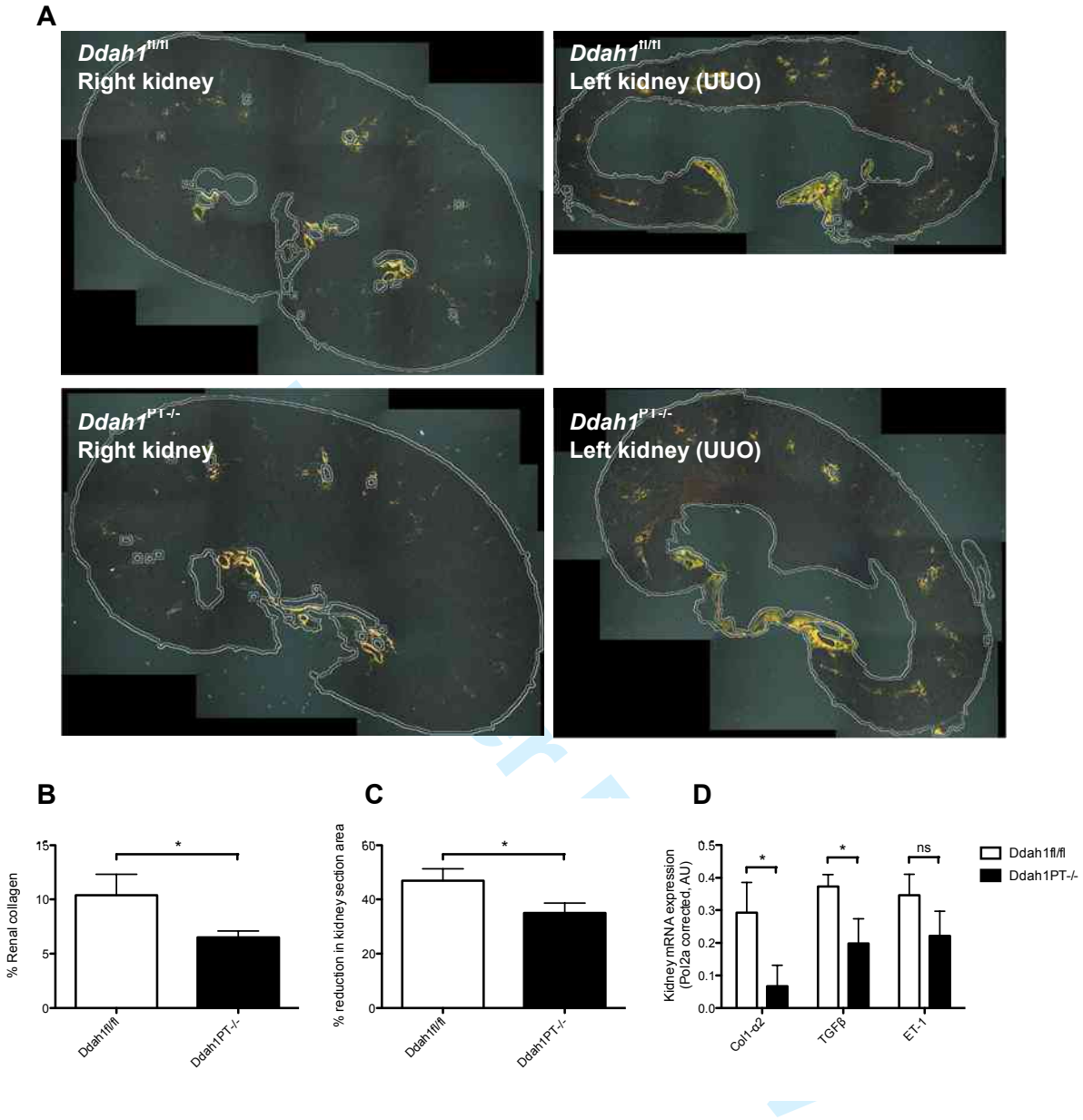

Figure 9. Effects of PT-specific DDAH1 deletion at two weeks following UUO

A and **B**, Renal collagen deposition was significantly lower in than *Ddah1*$^{fl/fl}$ controls (determined by non-biased software analysis of picrosirius red stained sections; 6.6 vs 10.4%; p<0.05). **C**, Renal parenchyma was less contracted in *Ddah1*$^{PT-/-}$ mice (assessed by percentage reduction of whole kidney section area (compared to unobstructed contralateral kidney in same mouse; 35 vs 47% in *Ddah1*$^{fl/fl}$ controls; p<0.05). **C,** RT-qPCR analysis revealed significantly lower renal tissue pro-fibrotic cytokine expression in *Ddah1*$^{PT-/-}$ mice. Collagen 1 subunit α2 (*Col1α2*) >4-fold (0.07 vs 0.29 AU in *Ddah1*$^{fl/fl}$ controls; p<0.05); transforming growth factor β (*TGFβ*) 2-fold (0.19 vs 0.37 AU in *Ddah1*$^{fl/fl}$ controls; p<0.05); and endothelin-1 (*ET-1*) by ~40% (0.22 vs 0.35 AU; not statistically significant). Mann-Whitney U test, n=13 (*Ddah1*$^{fl/fl}$) and n=20 (*Ddah1*$^{PT-/-}$). *p<0.05.

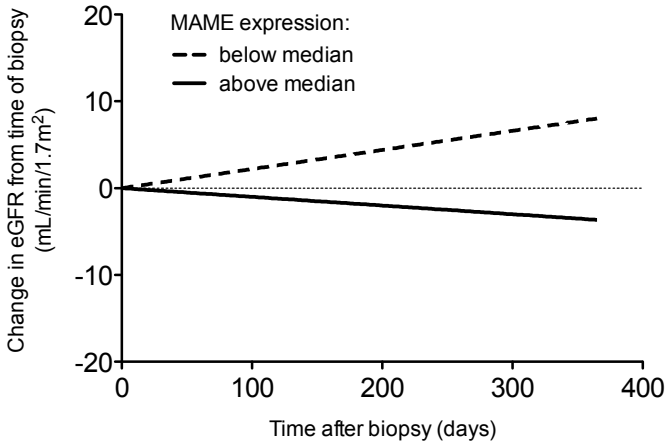

Figure 10. Relationship between kidney tissue MAME expression and eGFR decline in renal transplant recipients.
Estimates of [change in] eGFR over time in London cohort stratified by MAME expression (above or below median) derived from the multilevel model. Dotted line, MAME expression below median; solid line, MAME expression above median

Peer Review

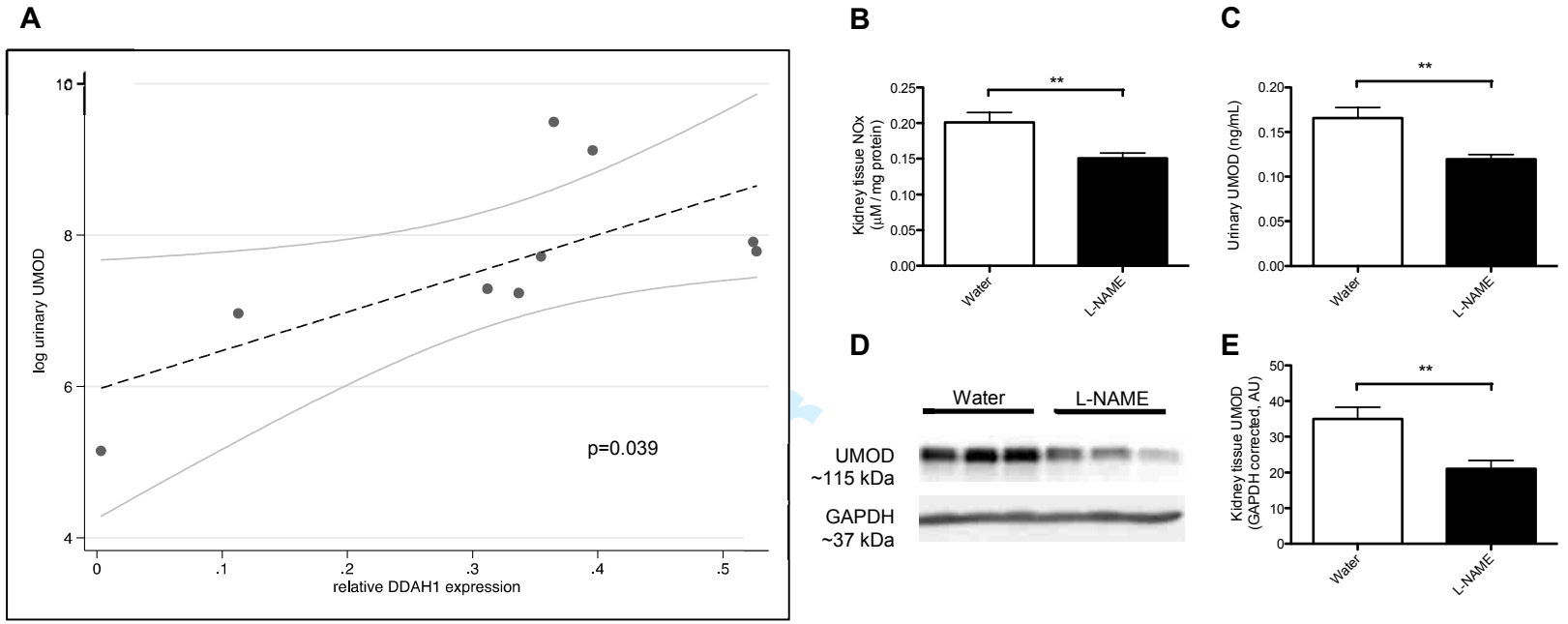

Figure 11. Relationship between DDAH1 gene expression, NO activity and UMOD protein expression
A, Renal biopsy tissue DDAH1 mRNA expression positively correlated with urinary UMOD in live donor allografts (p=0.039). When extended to the whole cohort, the association was rendered statistically insignificant which likely reflects the heterogeneity of organs from deceased donors. B – D, non-selective NOS inhibition with L-NAME dissolved in drinking water (1mg/mL for two weeks) in wild-type C57BL/6 mice. **B**, L-NAME-treated mice had significantly reduced kidney tissue NOx (p<0.01; determined by chemiluminescence) and significantly lower UMOD protein expression in urine (**C**, p<0.01; by ELISA) and kidney tissue (**D**,**E**, p<0.01; Western blot; n=3 representative of 8 in each group). Mann-Whitney U test. **p<0.01.

Supplementary material

1 HUMAN COHORT DATA

1.1 *DDAH1* alone

DD1	London			Virginia		
	Estimate	95%	CI	Estimate	95%	CI
GFR change over time mL/min/1.72m2 per day	0.023	0.005	0.041	0.011	-0.015	0.038
Increase in GFR at biopsy mL/min/1.72m2 per unit DD1	17.099	-5.043	39.241	17.738	8.972	26.503
Change in GFR over time per mL/min/1.72m2 per unit DD1 per day	-0.046	-0.091	0.000	-0.048	-0.101	0.005

Standard deviation of eGFR estimates: (i) between subject at baseline (intercept): London, 16.0ml/min per 1.73m^2 (95% CI, 12.6–20.2); Virginia, 14.1ml/min per 1.73m^2 (95% CI, 10.8-18.5); (ii) between subject over time (slope): London, 0.02ml/ min per 1.73m^2 per day (95% CI, 0.01–0.04); Virginia, 0.04ml/min per 1.73m^2 per day (95% CI, 0.03-0.05); (iii) within subject: London, 7.1ml/min per 1.73m^2 (95% CI, 6.7–7.5); Virginia, 7.3ml/min per 1.73m^2 (95% CI, 6.8–7.9). Correlation between baseline eGFR (intercept) and slope: London: 0.01 (95% CI, -0.48-0.50); Virginia: 0.18 (95% CI, -0.24-0.55).

1.2 *AGXT2* alone

AGXT2	London			Virginia		
	Estimate	95%	CI	Estimate	95%	CI
GFR change over time mL/min/1.72m2 per day	0.032	0.015	0.049	0.013	-0.012	0.038
Increase in GFR at biopsy mL/min/1.72m2 per unit MAME	13.221	-9.611	36.052	19.219	0.924	37.513
Change in GFR over time per mL/min/1.72m2 per unit MAME per day	-0.060	-0.096	-0.023	-0.045	-0.086	-0.003

Standard deviation of eGFR estimates: (i) between subject at baseline (intercept): London, 16.4ml/min per 1.73m^2 (95% CI, 12.9–20.8); Virginia, 16.1ml/min per 1.73m^2 (95% CI, 12.5-21.1); (ii) between subject over time (slope): London, 0.02ml/ min per 1.73m^2 per day (95% CI, 0.01–0.03); Virginia, 0.03ml/min per 1.73m^2 per day (95% CI, 0.02-0.05); (iii) within subject: London, 7.0ml/min per 1.73m^2 (95% CI, 6.6–7.5); Virginia, 7.3ml/min per 1.73m^2 (95% CI, 6.8–7.9). Correlation between baseline eGFR (intercept) and slope: London: 0.03 (95% CI, -0.50-0.54); Virginia: 0.11 (95% CI, -0.30-0.50)

For Peer Review

1.3 Plasma ADMA correlation with kidney tissue *DDAH1* expression

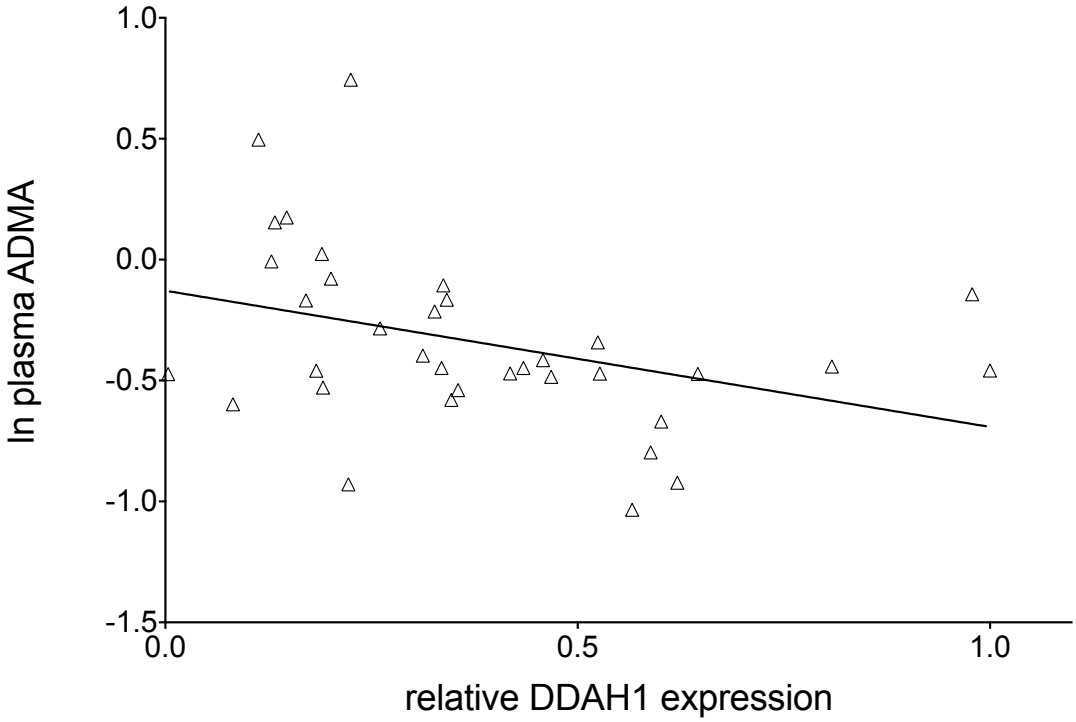

log_pl_adma	Coef.	Std. Err.	t	P>|t|	[95% Conf.	Interval]
reldd1	-.5633755	.2495867	-2.26	0.031	-1.071164	-.0555875
_cons	-.1283758	.1115929	-1.15	0.258	-.3554133	.0986617

2 CHARACTERISATION OF THE FOLATE NEPHROPATHY MODEL

2.1 Introduction

Folate (folic acid or pteroylglutamic acid) is an essential cofactor required for the synthesis of pyridines and pyrimidines to create DNA. Freely filtered at the glomerulus, folate is actively reabsorbed in the proximal tubule by specialised transport proteins (α-folate receptor proteins, α-FRs). [1] Supplementary oral folate is routinely prescribed for patients with ESRD on haemodialysis, malnourished patients, and pregnant women.

Administration of intraperitoneal (IP) folate is a well-established experimental technique to model renal injury. [2-4] When folate is administered in supra-therapeutic doses (180-240μg/g; ~15,000-fold higher than the 5mg daily prescribed dose in haemodialysis patients), folate crystals precipitate within renal tubule lumina and induce dose-dependent nephrotoxicity. Widespread acute tubular necrosis ensues within 48 hours with a concomitant rise in serum creatinine and BUN to mimic AKI. A period of epithelial regeneration follows, and from 2 weeks following injury, the kidneys exhibit progressive fibrosis and loss of function. Folate injury thus provides a reproducible model with which to examine the natural history of inflammation from initiating acute tubular injury through to slowly progressive fibrosis characteristic of chronic kidney disease.

Prior to adopting folate nephropathy as the model for CKD in this study, it was necessary to characterise the course of folate-induced renal disease and assess the quality of data that could be gained using a variety of analysis techniques.

2.2 Study design

Forty, 10-week old female WT C57BL6 littermate mice were purchased from Charles River Ltd (Kent, UK) and randomly assigned to receiving a single IP injection of either vehicle (0.3M $NaHCO_3$) or folate (240μg/g, dissolved in 0.3M $NaHCO_3$). Mice were sacrificed at 2 days, 2 weeks and 12 weeks. A detailed description of tissue harvesting can be found in the Methods chapter.

For Peer Review

Group sizes were between 5-8 (no premature deaths were experienced in this study).

2.3 Results

2.3.1 Kidney : body weight ratio and appearance

The kidney : body weight ratio changed appreciably over the course of the disease: initially increasing by 30% at day 2 (<0.0001) with a pale, swollen appearance (Figure 1A), followed by a return to baseline weight at 2 weeks (Figure 1B). At 12 weeks following folate injection, the kidneys had shrunk to 30% less than vehicle-treated controls with a pale, shrivelled appearance (Figure 1C).

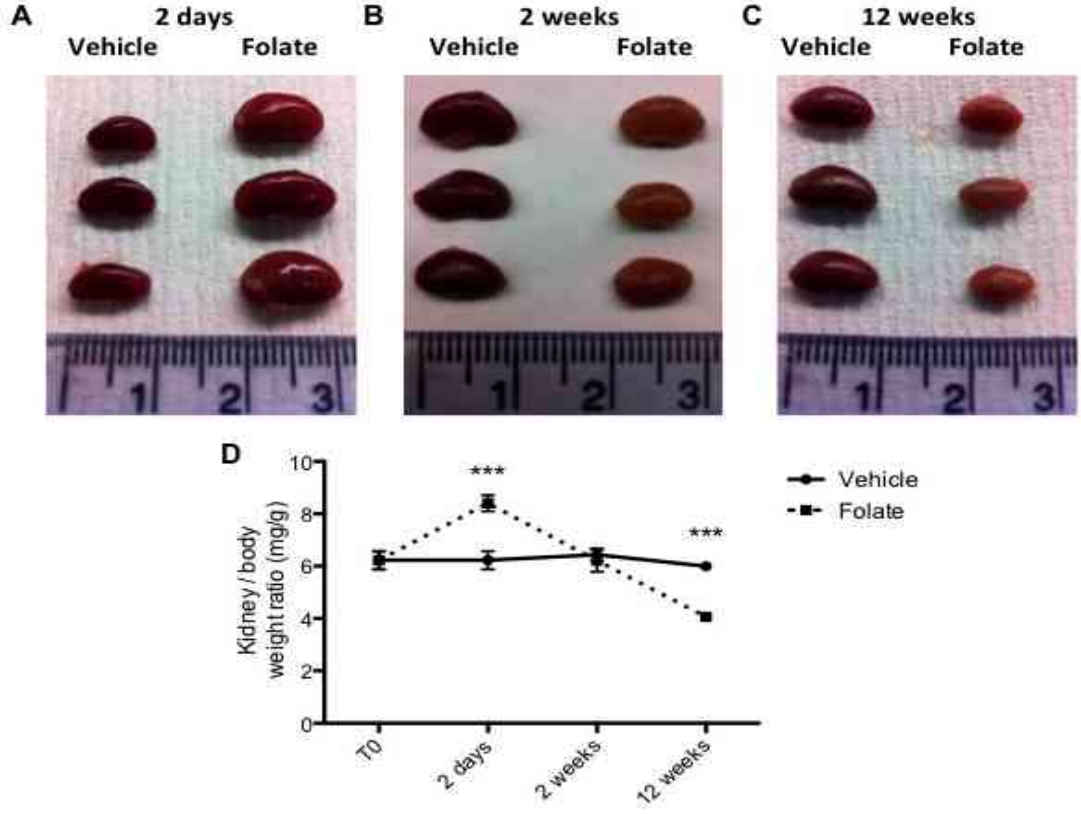

Figure 1. Kidney : body weight and appearance in folate nephropathy

Photographs of harvested kidneys (left-sided) following vehicle vs folate administration at (**A**) 2 days; 6.2 vs 8.4 mg/g (95% CIs 5.3-7.2 and 7.7-9.1); p<0.0001. (**B**) 2 weeks; both 6.2 mg/g. (**C**) 12 weeks; 6 vs 4.1 mg/g (95% CIs 5.6-6.4 and 3.7-4.4); p<0.0001. Three kidneys imaged to represent; vehicle-treated n=5; folate-treated n=8. (**D**) Graphical representation of kidney : body weight ratios (milligrams per gram, mg/g). Two-way ANOVA with Bonferroni's post test. n=5 (vehicle), n=8 (folate) ***p<0.0001.

2.3.2 Serum and urinalysis

At 2 days following folate administration, serum creatinine rose significantly (16-fold; p<0.001) over vehicle-treated animals, falling to 3-fold higher at 2 weeks (p<0.05) and remained 2-fold higher than controls at 12 weeks (p<0.05) (Figure 2).

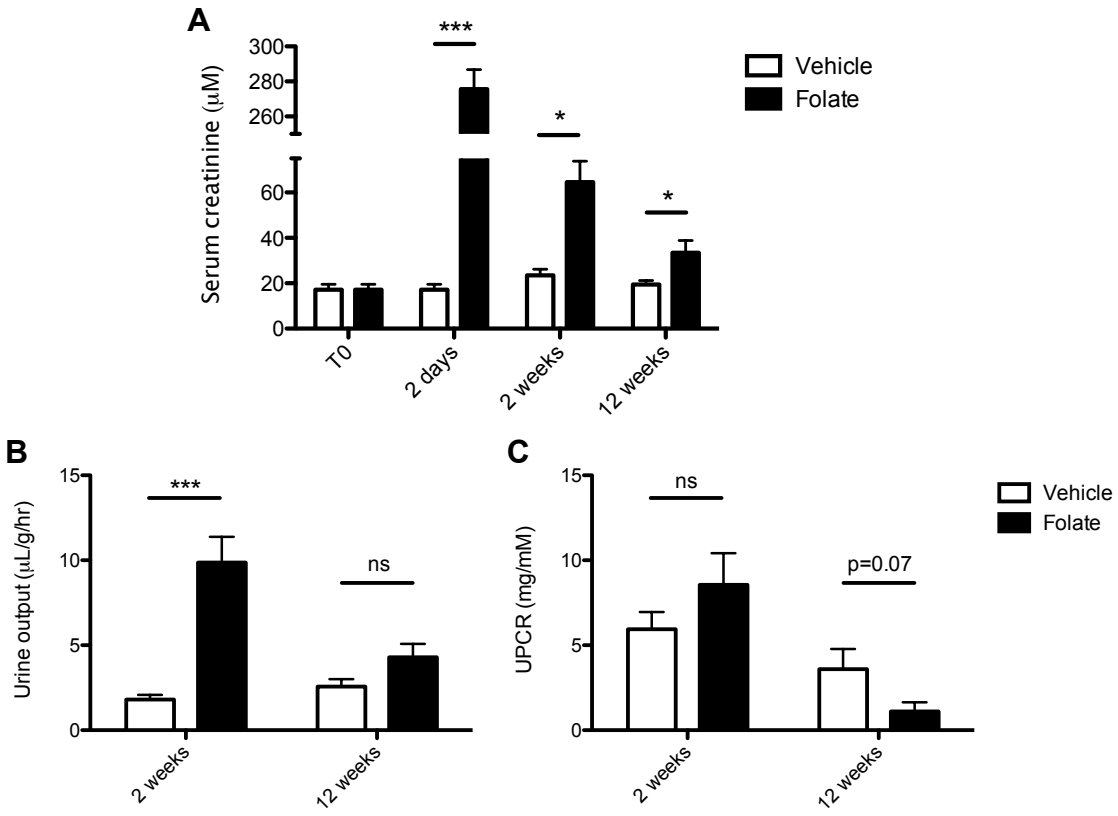

Figure 2. Serum creatinine (A), urine output (B) and proteinuria (C) in folate nephropathy

Serum creatinine was quantified by LC-MS/MS. (**A**) Serum creatinine (vehicle vs folate) at 2 days; 17 vs 276 μM (95% CIs 11-24 and 249-302); p<0.001. 2 weeks; 24 vs 65 μM (16-31 and 43-87); p<0.05. 12 weeks; 19 vs 34 μM (15-24 and 20-47); p<0.05. (**B**) Urine output was elevated at 2 weeks; 1.8 vs 9.9 mL/g/hr (1.2-2.5 and 6.5-13.3); p<0.001. (**C**) Proteinuria was raised at 2 weeks and fell by 12 weeks (not statistically significant between treatment groups). Two-way ANOVA with Bonferroni's post test. n=5 (vehicle), n=8 (folate). *p<0.05 ***p<0.001.

For humane reasons, housing mice in metabolic cages was avoided during the period of acute inflammation hence urinary data at 2 days are not available. Mice treated with folate displayed significant polyuria at 2 weeks (5-fold; p<0.001), which reduced to a level marginally above vehicle-treated controls at 12 weeks (non-significant). Proteinuria, reported as urinary protein-creatinine ratio did not significantly change at either time point.

2.3.3 MAME expression, MAs and NO activity

Kidney tissue mRNA expression of both DDAH isoforms (1 and 2) and AGXT2 was altered during the course of folate-induced kidney disease (Figure 3). DDAH1 expression was reduced at 2 and 12 weeks although this was not statistically significant. DDAH2 expression did not change until 2 weeks with ~3-fold upregulation ($p<0.001$), persisting at 12 weeks ($p<0.01$). AGXT2 expression fell 37-fold at 2 days following folate in comparison to vehicle treatment ($p<0.001$), recovering to baseline by 12 weeks.

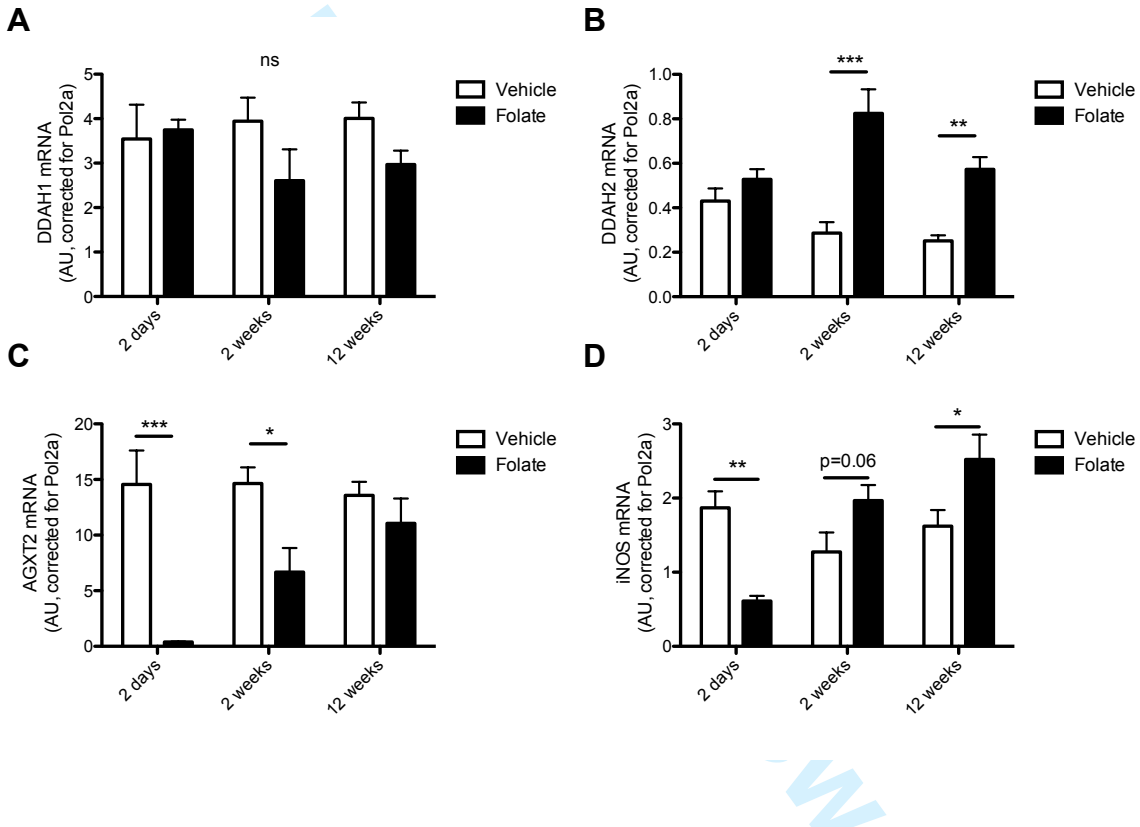

Figure 3. Whole kidney tissue MAME and *iNOS* expression in folate nephropathy

mRNA expression measured by RT-qPCR. (**A**) DDAH1 expression did not change significantly although there was a trend towards downregulation at 2 and 12 weeks following folate. (**B**) DDAH2, 2 weeks 0.3 vs 0.8 AU (95% CIs 0.2-0.4 and 0.5-1.2); $p<0.001$. 12 weeks 0.3 vs 0.6 AU (0.2-0.3 and 0.4-0.7); $p<0.01$. (**C**) AGXT2, 2 days 14.6 vs 0.4 AU (4.8-24.3 and 0.3-0.5); $p<0.001$. 2 weeks 14.7 vs 6.7 AU (10.6-18.7 and 1.4-12.0); $p<0.05$. 12 weeks, non-significant. Two-way ANOVA, *$p<0.05$, **$p<0.01$, ***$p<0.001$.

In response to folate renal injury, methylarginine concentrations in plasma, urine and whole kidney tissue changed over time (Figure 4). At 2 days, plasma L-NMMA and SDMA rose significantly in response to folate administration (8- and 4-fold respectively; $p<0.001$) and quickly fell towards baseline at 2 and 12 weeks. ADMA plasma concentrations did not alter at 2

days and although trended towards a rise at 2 and 12 weeks, did not increase significantly.

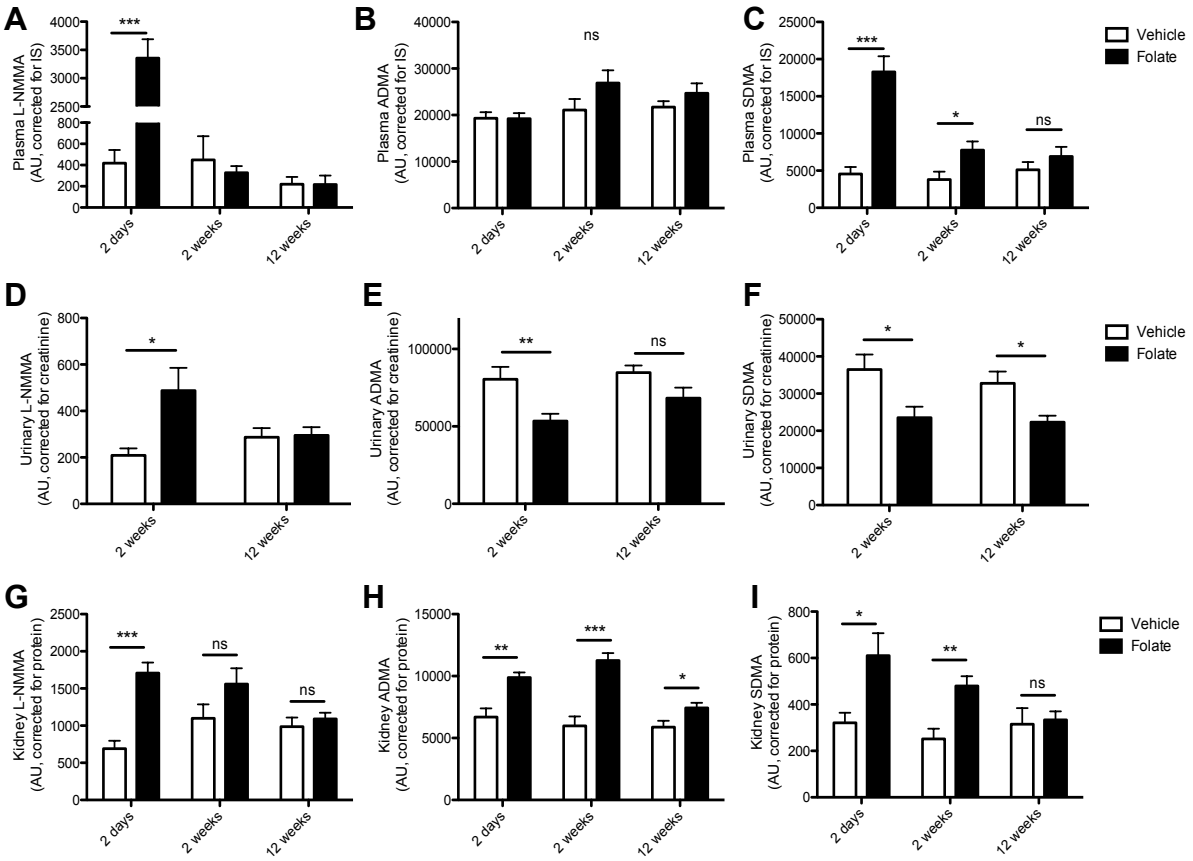

Figure 4. Methylarginine (MA) content in plasma, urine and whole kidney in folate nephropathy

MAs measured by LC/MSMS. (**A**) Plasma L-NMMA and (**C**) SDMA were elevated at 2 days. L-NMMA (vehicle vs folate), 418 vs 3356 AU (95% CIs 72-764 and 2566-4145); p<0.001. SDMA, 4551 vs 18290 AU (1925-22753 and 13310-23270); p<0.001. (**D**) Urinary L-NMMA at 2 weeks, 209 vs 488 AU (138-280 and 266-710); p<0.05. (**E**) Urinary ADMA at 2 weeks, 80415 vs 53466 AU (61529-99301 and 42868-64065); p<0.01. (**F**) Urinary SDMA at 2 weeks, 36500 vs 23530 AU (26990-46010 and 16860-30199); p<0.05, similar effect remained at 12 weeks. (**G**) Kidney L-NMMA was elevated at 2 days 690 vs 1707 (392-988 and 1371-2043); p<0.001 and fell to non-significantly elevated levels at 2 and 12 weeks. (**H**) Kidney ADMA was elevated at every time-point with a peak at 2 weeks, 5978 vs 11258 AU (3856-8100 and 9837-12679); p<0.001. (**I**) Kidney SDMA was most elevated at 2 days, 321 vs 557 AU (200-442 and 323-791); p<0.05 and fell to control levels by 12 weeks. Two-way ANOVA with Bonferroni's post test. n=5 (vehicle), n=8 (folate). *p<0.05, **p<0.01, ***p<0.001.

In urine, L-NMMA was elevated 2.5-fold (p<0.05) in folate-treated mice compared to vehicle controls but normalised at 12 weeks. Both urinary ADMA and SDMA were reduced in response to folate at 2 and 12 weeks (p<0.05).

Whole kidney content of all MAs increased by 1.5 to 2-fold at 2 days and 2 weeks ($p<0.05$-0.001) and fell towards baseline at 12 weeks, at which point the only MA being significantly elevated was ADMA (approximately 25%; $p<0.05$).

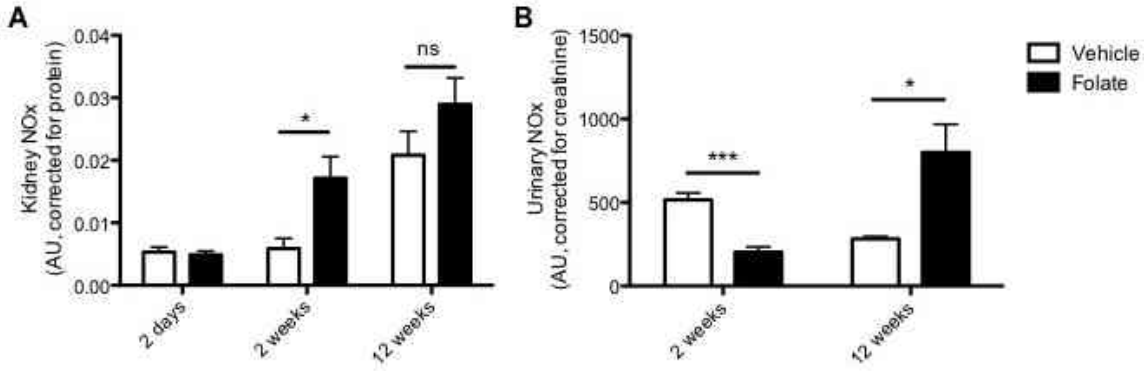

Figure 5. NOx concentrations in whole kidney and urine in folate nephropathy

NOx (nitrates and nitrites; stable end-products of NO activity) were measured by ozone chemiluminescence. (**A**) Kidney tissue NOx was unchanged at 2 days but rose significantly at 2 weeks, 0.006 vs 0.02 AU (0.0006-0.01 and 0.009-0.03); $p<0.05$. (**B**) Urinary NOx initially fell at 2 weeks but was increased at 12 weeks; 2 weeks 515 vs 204 AU (416-615 and 134-273); $p<0.001$.12 weeks 282 vs 800 AU (241-323 and 387-1213); $p<0.05$. Two-way ANOVA with Bonferroni's post test. n=5 (vehicle), n=8 (folate). *$p<0.05$, **$p<0.01$, ***$p<0.001$. (NOTE: The measurement of urinary NOx is not necessarily an accurate determination of renal NOS activity, particularly in the context of a nitrate-containing diet).

2.3.4 Acute inflammatory cytokines

Pro-inflammatory and pro-fibrotic cytokine mRNA transcription was up-regulated in whole kidney lysates with specific patterns over the three time-points (Figure 6). The most acute responses were exhibited by ET-1 and IL6, with transcription peaks at 2 days (5-fold and 25-fold respectively; $p<0.001$) before falling towards baseline at 2 and 12 weeks. TNFα mRNA transcription was delayed in comparison, with no change at 2 days and a 7-fold peak at 2 weeks ($p<0.001$) with a reduced but significant elevation persisting at 12 weeks ($p<0.01$). Housekeeper Pol2a transcription did not significantly change at any time point.

For Peer Review

2.3.5 Pro-fibrotic cytokines

Pro-fibrotic cytokines; TGFβ and Col1 2α were up-regulated acutely at 2 days but peaked at 2 weeks (3- and 12-fold respectively) and mRNA transcription remained significantly elevated at 12 weeks (Figure 6D-E).

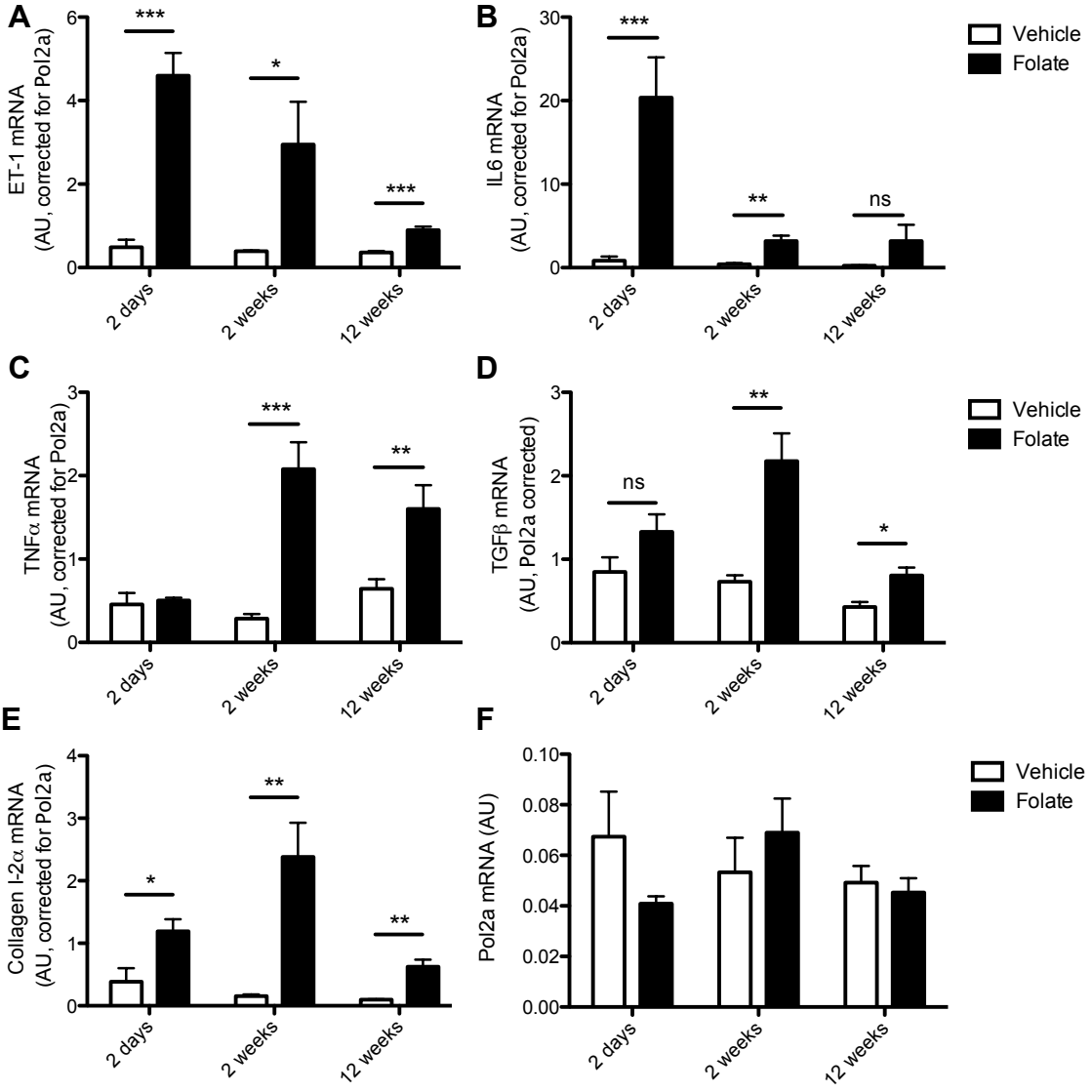

Figure 6. Whole kidney tissue mRNA transcription of pro-inflammatory (A-C) and pro-fibrotic (D, E) cytokines in folate nephropathy

mRNA transcription measured by RT-qPCR. Vehicle vs folate: (**A**) ET-1 (endothelin-1); 2 days 0.5 vs 4.6 AU (95% CIs -0.09-1.1 and 3.3-5.9); p<0.001. 2 weeks 0.4 vs 2 AU (0.3-0.5 and 0.8-3.2); p<0.05. 12 weeks 0.4 vs 0.9 AU (0.3-0.5 and 0.7-1.1); p<0.001; (**B**) IL6 (interleukin-6); 2 days 0.8 vs 20 AU (-0.7-2.4 and 8.9-31.8); p<0.001. 2 weeks 0.4 vs 3.2 AU (-0.02-08 and 1.6-4.8); p<0.01. 12 weeks 0.2 vs 3.2 AU (0.1-0.4 and -1.8-8.2); p>0.05. (**C**) TNFα (tumour necrosis factor-α); 2 weeks 0.3 vs 2.1 AU (0.1-0.4 and 1.3-2.9); p<0.001. 12

weeks 0.7 vs 1.6 AU (0.4-0.9 and 0.9-2.3); p<0.01. (**D**) TGFβ (transforming growth factor-β); 2 weeks 0.7 vs 2.2 AU (0.5-0.9 and 1.4-3.0); p<0.01. 12 weeks 0.4 vs 0.8 AU (0.3-0.6 and 0.6-1.0); p<0.05. (**E**) Col12α (Collagen1 subunit 2α); 2 days 0.4 vs 1.2 AU (-0.3-1.1 and 0.7-1.6); p<0.05. 2 weeks 0.2 vs 2.4 AU (0.1-0.2 and 1.1-3.7); p<0.01. 12 weeks 0.1 vs 0.6 AU (0.08-0.1 and 0.3-0.9); p<0.01. (**F**) Housekeeper Pol2a transcription did not change. Two-way ANOVA with Bonferroni's post test. n=5 (vehicle), n=8 (folate). *p<0.05, **p<0.01, ***p<0.001.

2.3.6 Histological features

Severe tubulointerstitial disease was evident in kidney sections from folate-treated mice (Figure 7). At 2 days; tubular dilatation and epithelial flattening, luminal casts; tubular atrophy. At 2 weeks; interstitial inflammatory cell infiltrates and 12 weeks; tubular atrophy and areas of extra-cellular matrix deposition. Vehicle-treated mice displayed normal histological appearances at all time points.

2.3.7 Renal fibrosis (collagen deposition)

Collagen deposition quantified by picrosirius red immunostaining was significantly elevated in animals treated with folate at 2 and 12 weeks (vehicle vs folate: 2 weeks, 4 vs 5.7%, p<0.01; 12 weeks, 2.7 vs 6.4%, p<0.001). Figure 8).

For Peer Review

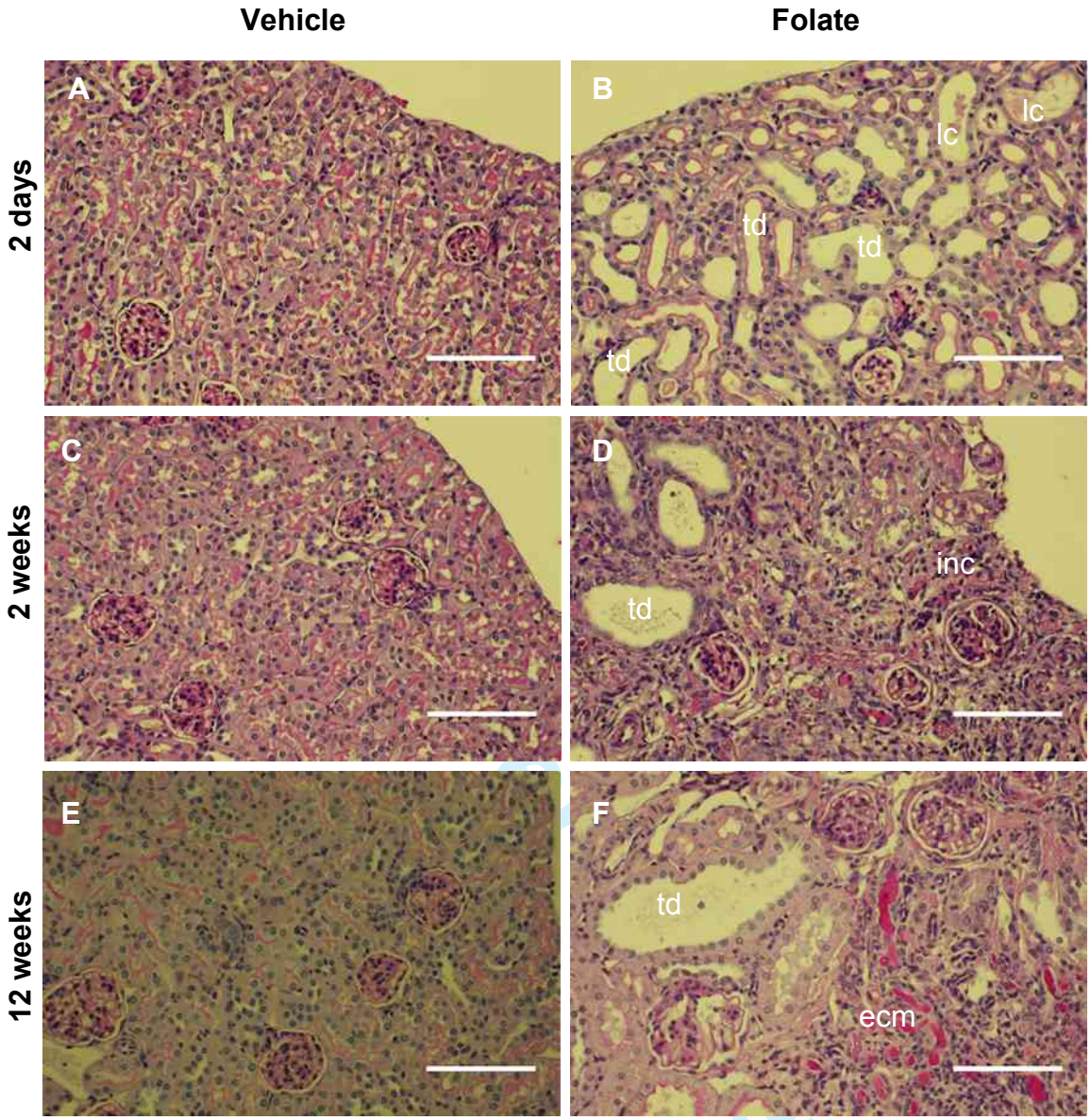

Figure 7. Representative histological features of folate nephropathy

A, C and E: vehicle controls displayed normal histological appearances; dense with tubules, their lumina barely visible. **B, D and F:** folate-treated mice at 2 days, 2 and 12 weeks respectively. Gross and diffuse tubular dilatation (**td**) with some luminal casts (**lc**) was visible at 2 days (**B**). Some resolution of tubular dilatation was apparent at 2 weeks (**D**), but with added presence of interstitial inflammatory cells (**inc**) (darker nuclei). By 12 weeks (**F**), some earlier features remained but with marked expansion of extra-cellular matrix (**ecm**), tubular atrophy and some glomerulosclerosis seen lower left quadrant. Representative of n=5 (PBS vehicle) and n=8 (folate). PAS stain, x20 magnification. Bars = 50 μm.

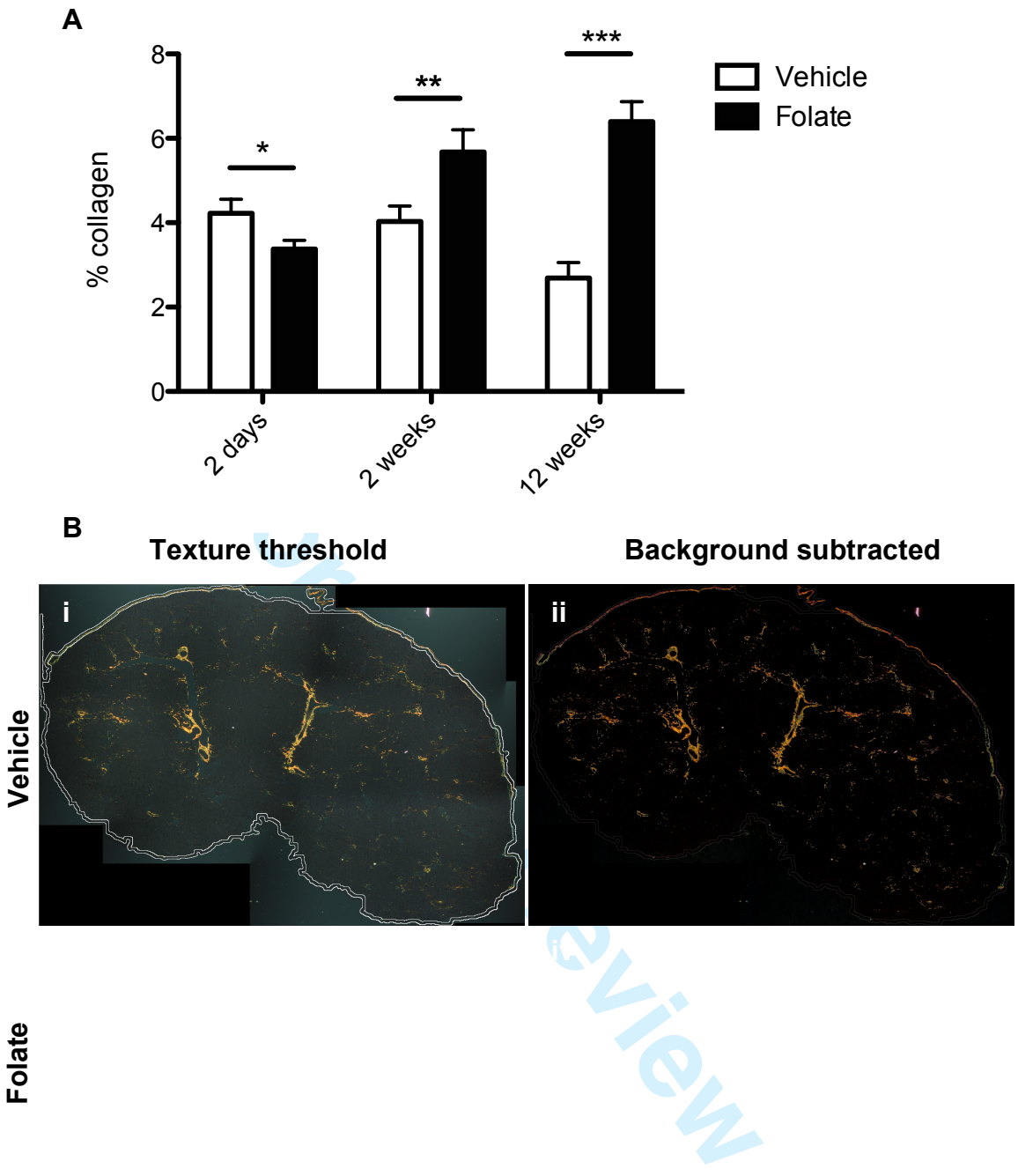

Figure 8. Renal collagen deposition in folate nephropathy

Representational images of kidney sections from mice treated with (**i-ii**) **Vehicle** and (**iii-iv**) **Folate**. Stained with picrosirius red and viewed through circularly polarised light. A detailed description of this method, developed with the assistance of Dr Dorman (MRC CSC, London), is reported in the Methods section. Section area defined through **texture thresholding** (**i** and **iii**). Capsular collagen was excluded from the analysis by automated circumferential reduction of the analysed perimeter (double lines). Background is **subtracted** to measure percentage collagen per total section area (**ii** and **iv**). (**G**) Percentage collagen deposition is significantly elevated at 2 and 12 weeks. 2 weeks (vehicle vs folate); 4.0 vs 5.7% (95% CIs 3.0-5.1 and 4.4-6.9); $p<0.01$. 12 weeks; 2.7 vs 6.4% (1.7-3.7 and 5.2-7.6); $p<0.001$. Two-way ANOVA with Bonferroni's post test. n=5 (vehicle), n=8 (folate). *$p<0.05$, **$p<0.01$, ***$p<0.001$.

3 CHARACTERISATION OF THE UNILATERAL URETERIC OBSTRUCTION (UUO) NEPHROPATHY MODEL

3.1 Introduction

Unilateral ureteric obstruction in experimental animals has been used to examine mechanisms of human kidney disease for over fifty years and has become a well-established rodent model of renal fibrosis. [5] Within hours of ureteric ligation, renal blood flow and glomerular filtration rate decline rapidly as progressive hydronephrosis develops to cause tubular cell death, inflammatory cell infiltration and significant fibrosis within seven days. [6]

Advantages over other models include rapid and reproducible development of disease, the absence of an exogenous nephrotoxin with potential confounding effects and the use of the contralateral kidney as a control (although compensatory change in response to UUO has to be considered). Disadvantages include the additional skill and resource required for recovery surgery, the absence of a systemic "uraemic state" to model human CKD, and reduced or absent biomarkers of disease severity such as serum creatinine or proteinuria from the affected kidney.

Prior to adopting this method, it was important to characterize the UUO model to understand the natural course of injury and assess the quality of data obtained from this model.

3.2 Study design and methods

Thirty, 10-week old female WT C57BL6 littermate mice purchased from Charles River Ltd (Kent, UK) were randomly assigned to either unilateral ureteric obstruction or sham surgery (4 and 6 mice in each treatment arm respectively). Under isoflurane inhalation anaesthesia, mice were shaved, draped and positioned on a heat mat. In the supine position, a left flank incision exposed the left ureter and was ligated twice with 4-0 nylon sutures and transected. Following suture closure, animals received intramuscular diclofenac analgesia (Vetagesic) and recovered in heated chambers. No surgical complications or premature deaths were experienced in this study.

For Peer Review

Mice were sacrificed by cervical dislocation followed by organ harvesting at three time points; 1, 2 and 3 weeks.

3.3 Results

3.3.1 Kidney appearance

Significant hydronephrosis featuring marked pale discoloration of thinning of the renal parenchyma was evident at all time points from week 1 into week 3, (Figure 9).

Figure 9. Typical appearance of kidneys in the UUO nephropathy model

Pictured are those harvested at 2 weeks following UUO. The left obstructed kidney is grossly dilated following complete obstruction.

3.3.2 Serum creatinine

Serum creatinine has previously been reported to be unaffected in the UUO model, [7] however serum creatinine was raised in this study at each time-point, but significantly at 3 weeks by 70% in UUO-treated mice ($p<0.001$; Figure 10). This reflects an inability of the contralateral kidney to adequately compensate. Reasons for this are unclear. Mice were not exposed to additional systemic or renal compromise and it may reflect differences between strains (C57 strain used here) or even different genetic ancestry within strains.

For Peer Review

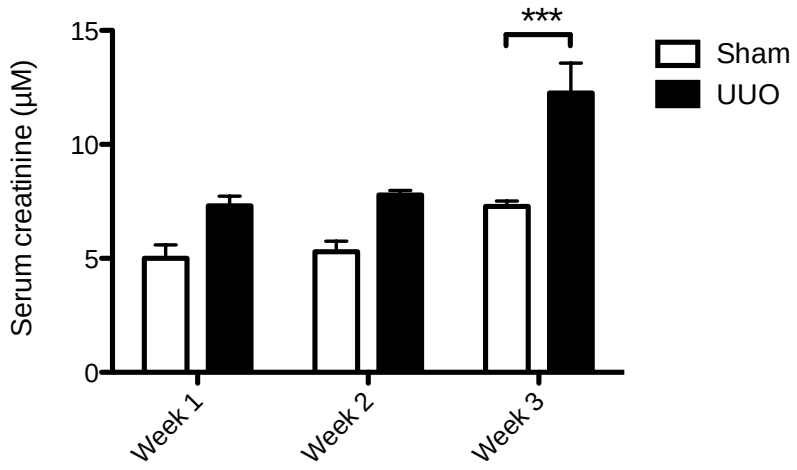

Figure 10. Serum creatinine following UUO

Serum creatinine quantified by LC-MS/MS. Sham versus UUO-treated; 7.3 vs 12.3 µM; p<0.001; (95% CI 2.2-7.7).Two-way ANOVA with Bonferroni's post test. n=4 (sham), n=6 (UUO). ***p<0.001

3.3.3 Physiological parameters

At 1 week following surgery, body weight fell 2-fold in UUO mice versus sham controls (Figure 11A). At 2 weeks, body weights recovered towards pre-surgical baselines although a trend for lower weight remained in UUO-treated mice. No significant differences in urine output between sham- and UUO-treated mice were observed although a trend for higher values in UUO mice is consistent with adaptive hyperfiltration in the contralateral kidney (Figure 11B). No significant systemic blood pressure differences were observed at any time point (Figure 11C), consistent with previous reports of UUO being a normotensive model of nephropathy. [7]

For Peer Review

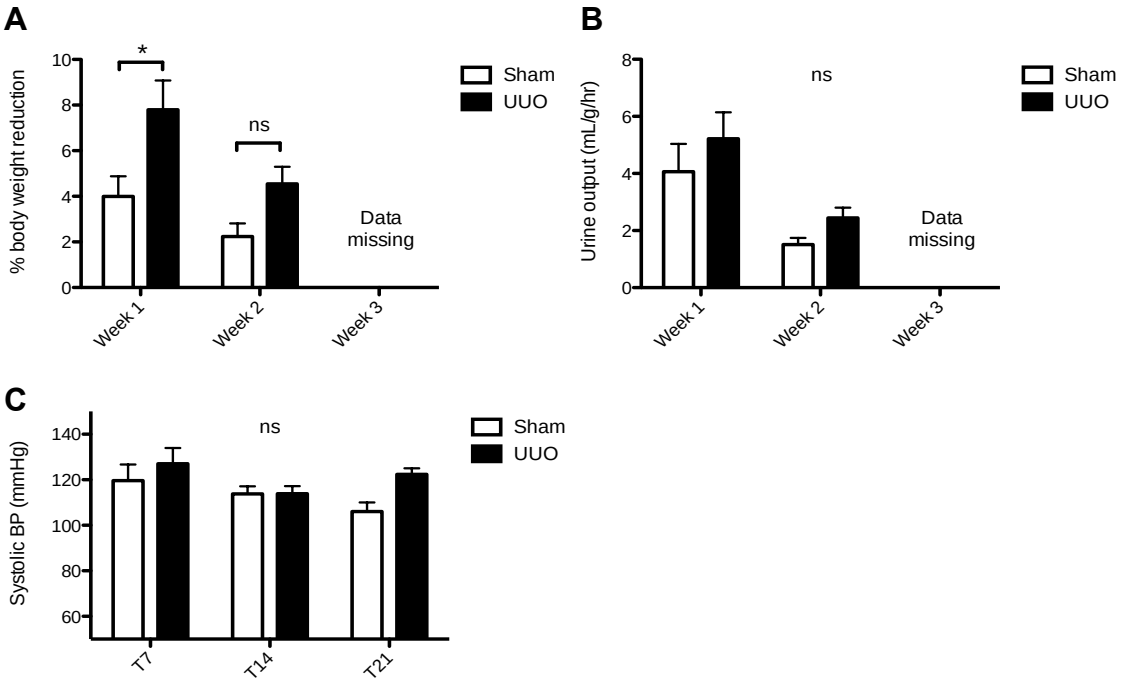

Figure 11. Body weight change, urine output and systolic blood pressure following UUO

(**A**) Percentage body weight reduction from pre-surgical baseline at 1 and 2 weeks following UUO. UUO-treated mice had a two-fold higher weight loss at 1 week than sham-operated controls (Sham versus UUO-treated; 3.99 vs 7.79%; $p<0.05$ (95% CI 0.27-7.3). No significant differences in urine output (**B**) or systolic BP (**C**) at any time point. Two-way ANOVA with Bonferroni's post test. n=4 (sham), n=6 (UUO). *$p<0.05$

3.3.4 Profibrotic and inflammatory cytokines

Expression of profibrotic (TGFβ, Col1α2 and ET-1; 17 - 21-fold) and pro-inflammatory (IL-6 and TNFα) genes was significantly increased in kidney tissues from UUO-treated mice when compared to sham-treated controls (Figure 12). Peaks in gene expression occurred at 2 – 3 week time-points with the exception of ET-1 (1 week).

Peer Review

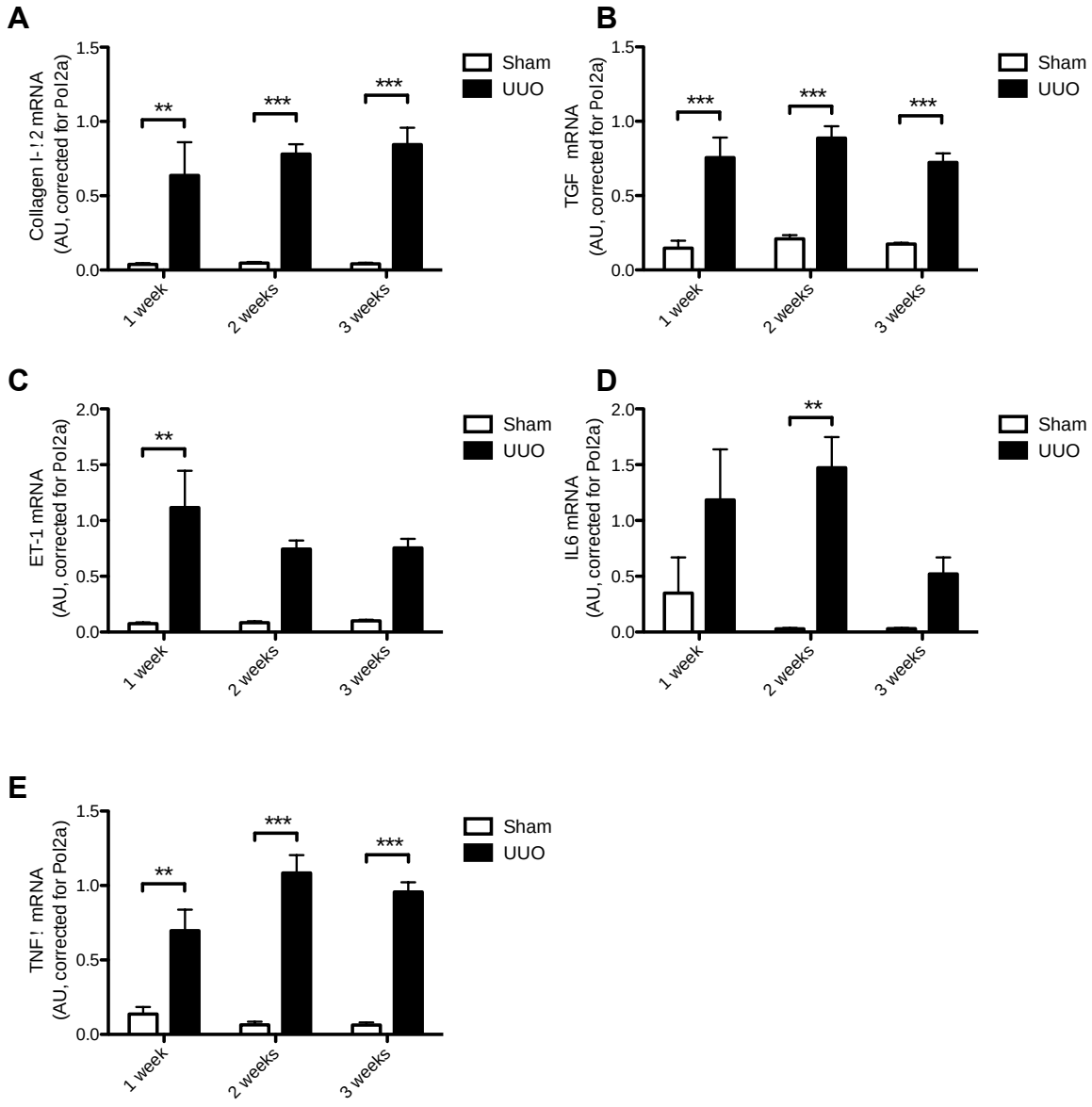

Figure 12. Kidney tissue profibrotic and inflammatory gene expression following UUO

mRNA transcription measured by RT-qPCR. Col12α (Collagen1 subunit 2α); TGFβ (transforming growth factor-β ET-1 (endothelin-1); IL6 (interleukin-6); TNFα (tumour necrosis factor-α); Two-way ANOVA with Bonferroni's post test. n=4 (sham), n=6 (UUO). **p<0.01, ***p<0.001

3.3.5 Methylarginine-metabolising enzymes (MAMEs)

Expression of methylarginine-metabolising enzyme (MAMEs; DDAH1, DDAH2 and AGXT2) genes in obstructed kidney tissue was significantly altered in the UUO model (Figure 13). DDAH1 (1 week 2-fold; 2 weeks 7-fold; 3 weeks 15-fold) and AGXT2 (1 week 2-fold; 2 weeks 6-fold; 3 weeks 25-fold) gene expression was progressively reduced, whilst DDAH2 expression was elevated 2 – 3-fold at each time-point.

These altered expression profiles reflect their cell-type specific expression. DDAH1 and AGXT2 in the kidney are known to be almost exclusively expressed within the tubular epithelium, [8] whilst DDAH2 is known to be induced within the macrophage by an inflammatory stimulus (our own findings; paper in submission). The UUO model causes widespread tubular damage and hence a large proportion of DDAH1/AGXT2-expressing cells are lost. How DDAH1 expression from surviving tubular cells affects progressive fibrosis forms the basis for this body of work.

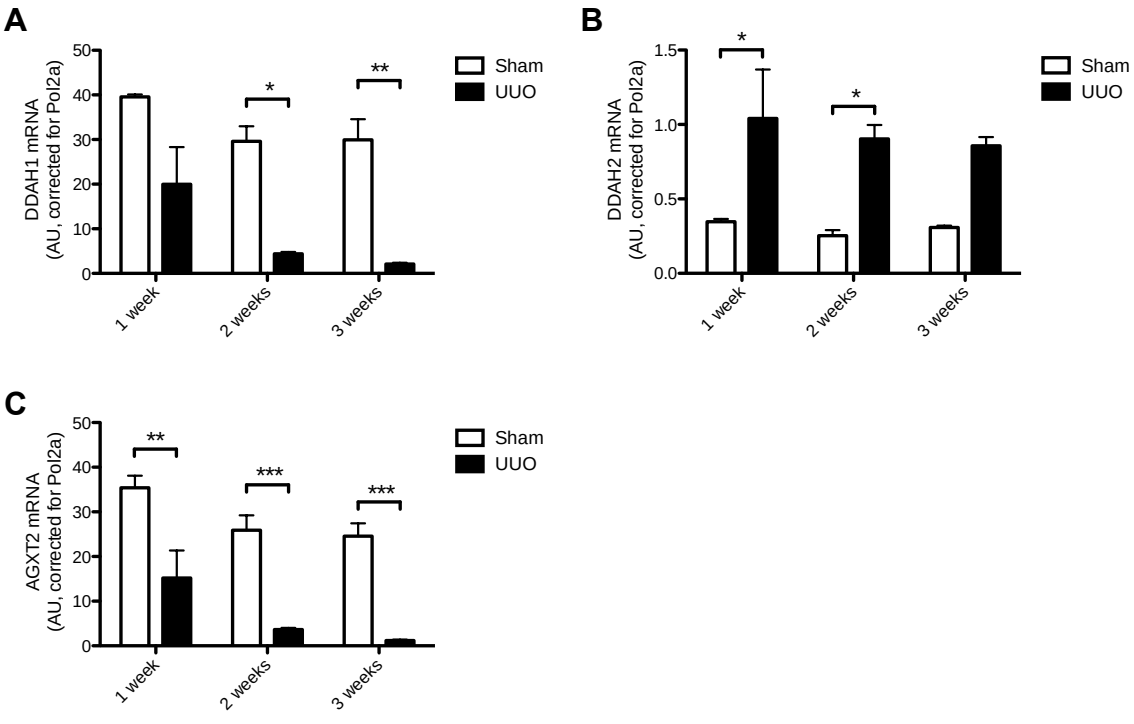

Figure 13. Kidney tissue methylarginine-metabolising enzyme (MAME) expression following UUO

mRNA transcription in kidney tissue measured by RT-qPCR. Two-way ANOVA with Bonferroni's post test. n=4 (sham), n=6 (UUO). *p<0.05, **p<0.01, ***p<0.001

3.3.6 Methylarginines

Asymmetric methylarginines (MAs), L-NMMA and ADMA, are metabolised by DDAH whilst SDMA is not. AGXT2 can metabolise all three through deamination. Few significant alterations in MAs were detected in the serum, kidneys and urine in the UUO model (Figure 14). All three MAs are known to rise in the serum or plasma in renal dysfunction[8] - a pattern reflected in this study. As yet, very little is understood about the role of MAs, MAMES and NO at a cell-type specific level in kidney function decline.

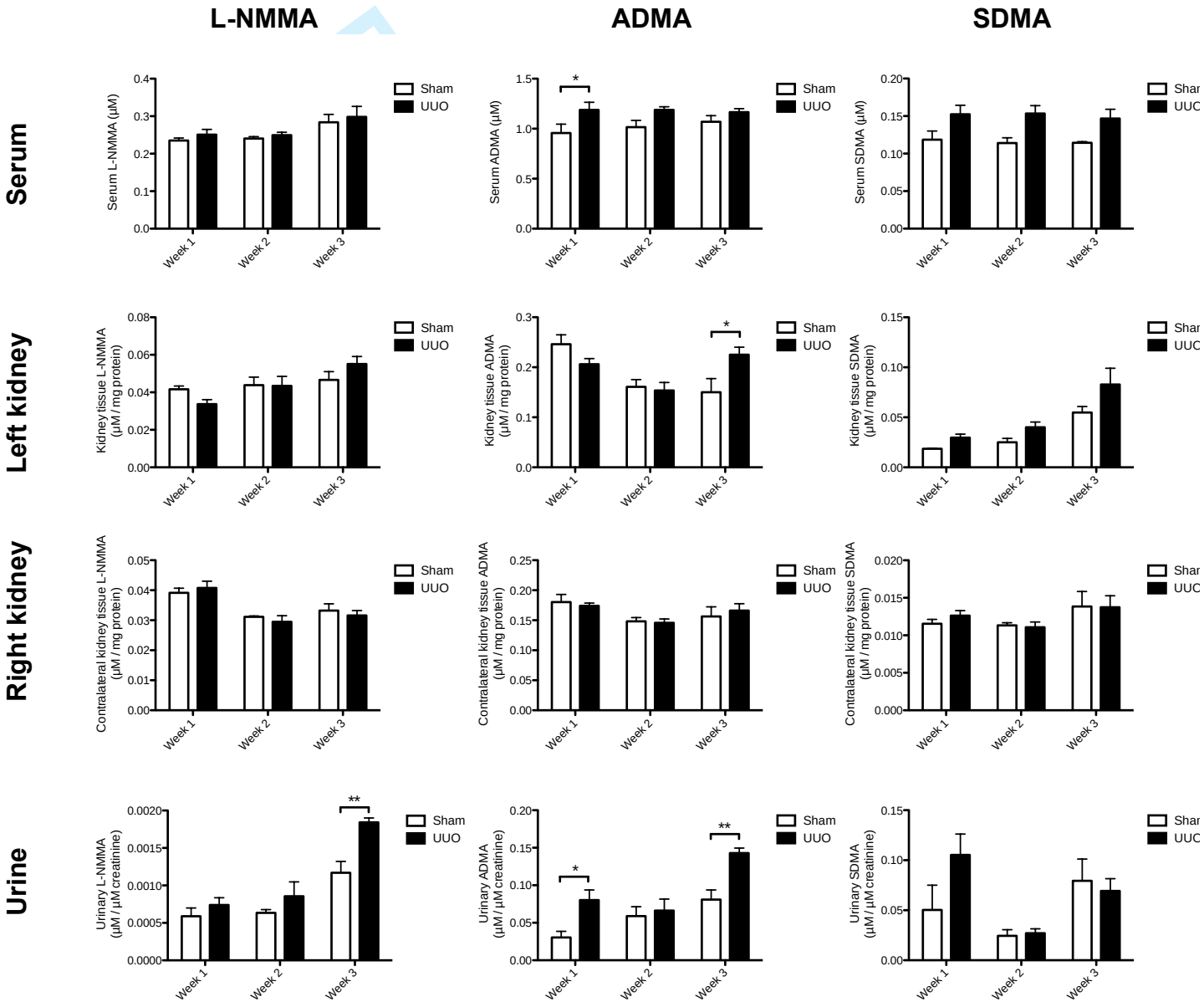

Figure 14. Methylarginine profiles following UUO

MAs measured by LC/MSMS. Two-way ANOVA with Bonferroni's post test. n=4 (sham), n=6 (UUO). *p<0.05, **p<0.01.

3.3.7 Nitric oxide concentrations

Evidence of nitric oxide activity assessed by quantification of stable end products (nitrite and nitrate; NOx). Plasma and urine NOx was not significantly altered following UUO at any time point (Figure 15A-B). Obstructed kidney tissue NOx was elevated at 2 weeks but only significant at 3 weeks (2-fold; $p<0.05$; Figure 15C), reflecting induced inflammation and increased NO production from immune cells. Interestingly, tissue from the contralateral kidney expressed a consistent pattern for reduced NOx, suggesting that part of the adaptive change exhibited by the single functioning kidney involves suppression of NO (Figure 15D).

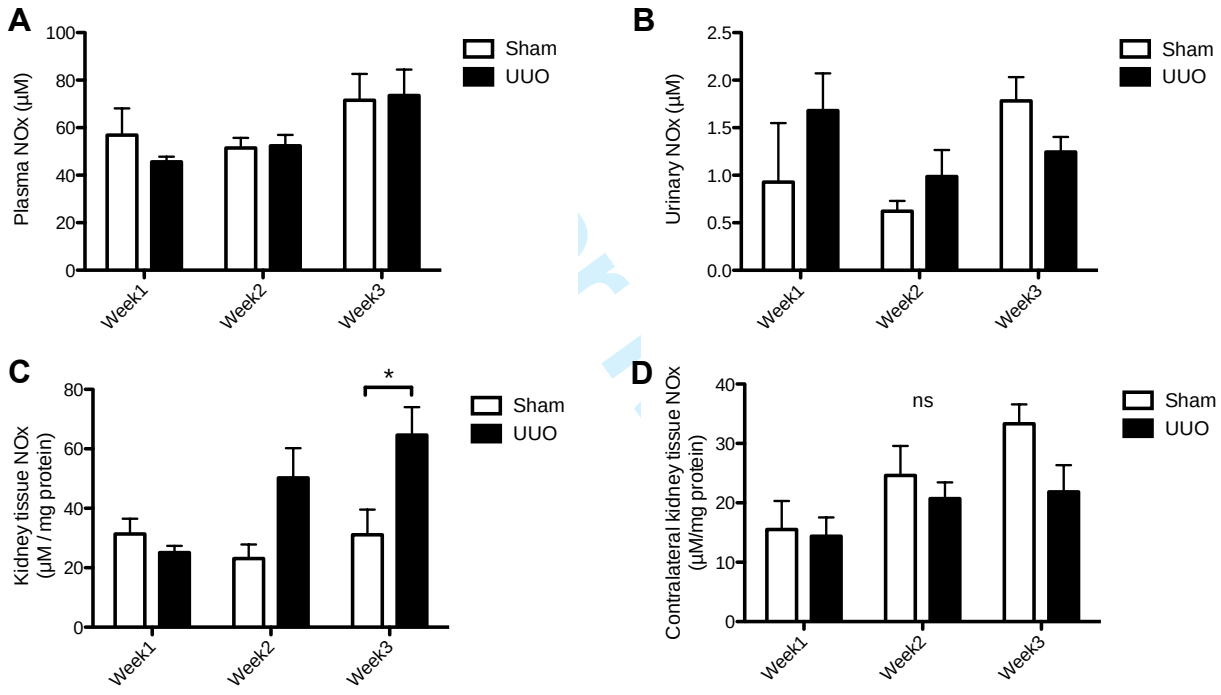

Figure 15. Nitric oxide (NO) activity following UUO

NOx (nitrates and nitrites; stable end-products of NO activity) measured by ozone chemiluminescence. (**A**) Two-way ANOVA with Bonferroni's post test. n=4 (sham), n=6 (UUO). *p<0.05. (NOTE: The measurement of urinary NOx is not necessarily an accurate determination of renal NOS activity, particularly in the context of a nitrate-containing diet).

3.3.8 Histology

Severe tubulointerstitial disease was evident in kidney sections from obstructed kidneys. At each time-point, gross tubular dilatation and epithelial flattening was present with luminal casts (Figure 16).

Figure 16. Renal histology following UUO

Tissue from sham operated displayed normal histological appearances; dense tubules, their lumina barely visible. **In obstructed kidneys;** gross, diffuse tubular dilatation (**td**) with some luminal casts (**lc**) evident at all time-points. Some resolution of tubular dilatation was apparent at 3 weeks with increased presence of interstitial inflammatory cells (**inc**) (darker nuclei) and marked expansion of extra-cellular matrix (**ecm**). Severe parenchymal thinning at 3 weeks allowing visualisation of the whole thickness in one frame (bottom-right image; pelvis and periphery labelled). Representative of n=4 (sham) and n=6 (UUO). PAS stain, x20 magnification. Bars = 50 μm.

For Peer Review

By 2 into 3-week time-points, tubular atrophy occurred with progressive interstitial inflammatory cell infiltration and areas of extra-cellular matrix deposition. At 3 weeks, marked thinning of the entire renal parenchyma (cortex and medulla) was evident with renal pelvis dilatation and further distortion of normal architecture (Figures 16 and 17). Sham-operated mice displayed normal histological appearances at all time points.

3.3.9 Renal fibrosis and loss of parenchyma

Progressive thinning of the renal parenchyma was evident throughout the time-course of UUO (Figure 17). Complete ureteric obstruction caused significant loss of whole kidney histological section surface area compared to sham-operated controls (55% reduction at 3 weeks; $p<0.001$; Figure 17A).

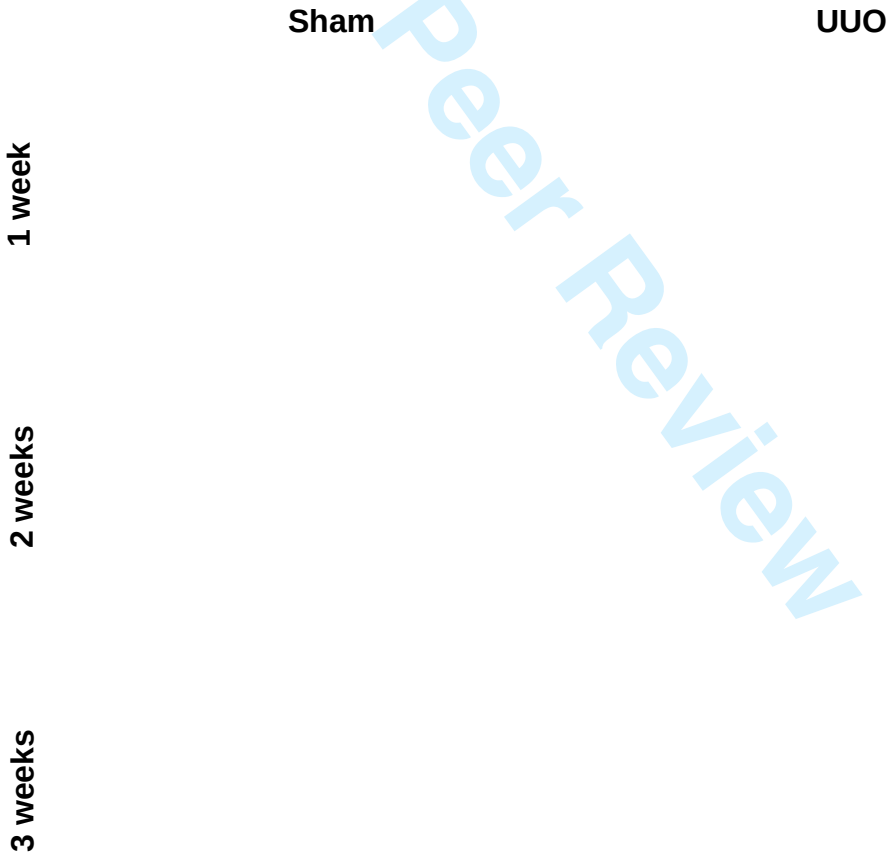

Figure 17. Renal fibrosis and parenchymal loss following UUO

Representational images of left kidney sections from mice following with sham or UUO surgery. Stained with picrosirius red and viewed through circularly polarised light. A detailed description of this method is reported in the Methods section. Section area defined through texture thresholding. Capsular collagen was excluded from the analysis by automated

For Peer Review

circumferential reduction of the analysed perimeter (double lines). Background is subtracted to measure percentage collagen per total section area (graphical representation; Figure 18A). Grossly distorted section morphology with dilated renal pelvis and parenchymal thinning evident at 2 and 3 week time-points.

Significant renal fibrosis or collagen deposition was evident in obstructed kidneys (12%; p<0.001; Figure 18B).

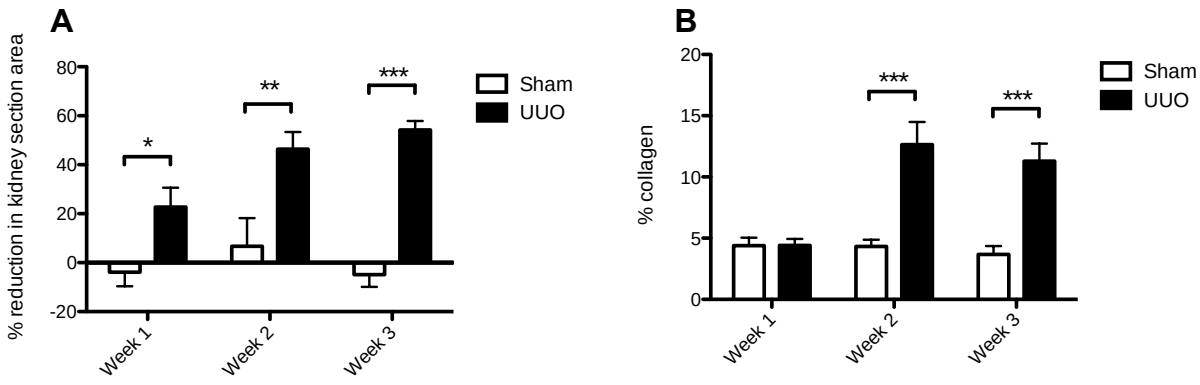

Figure 18. Reduced renal parenchyma and fibrosis.

Kidney section area assessed by reduction in pixel coverage in stitched whole kidney images as seen in Figure 13. Percentage collagen deposition quantified across whole kidney sections stained with picrosirius red and automated Image J software analysis. Two-way ANOVA with Bonferroni's post test. n=4 (sham), n=6 (UUO). *p<0.05, **p<0.01, ***p<0.001.

Peer Review

References

1 Kamen, B. A. & Caston, J. D. Identification of a folate binder in hog kidney. *! "#$%& ' ( ) *+$&,$-.&+&/.0*+$0"#1.23(4* ! "#, 2203-2205,(1975).

2 Mullin, E. M., Bonar, R. A. & Paulson, D. F. Acute tubular necrosis. An experimental model detailing the biochemical events accompanying renal injury and recovery. *5)6#237$8(&+7* $%, 289-294,(1976).

3 Koziolek, M. J., Muller, G. A., Zapf, A., Patschan, D., Schmid, H., Cohen, C. D., Koschnick, S., Vasko, R., Bramlage, C. & Strutz, F. Role of CX3C-chemokine CX3C-L/fractalkine expression in a model of slowly progressive renal failure. *9#:"(&+&/4;$ <.*+42.2;$ 3(*)2:+*)3*3.&)$ =$ &,,.0.*+$:'-+.0*3.&)$ &,$ 3"#$ >'(&:#*)$?.*+42.2$*)<$!(*)2:+*)3$@22&0.*3.&)A>'(&:#*)$B#)*+$@22&0.*3.&)* ! ", 684-698,(2010).

4 Long, D. A., Price, K. L., Ioffe, E., Gannon, C. M., Gnudi, L., White, K. E., Yancopoulos, G. D., Rudge, J. S. & Woolf, A. S. Angiopoietin-1 therapy enhances fibrosis and inflammation following folic acid-induced acute renal injury. *C.<)#4$5)37* &', 300-309,(2008).

5 Eddy, A. A., Lopez-Guisa, J. M., Okamura, D. M. & Yamaguchi, I. Investigating mechanisms of chronic kidney disease in mouse models. *D#<.*3(7$9#:"(&+7* !&, 1233-1247,(2012).

6 Chevalier, R. L., Forbes, M. S. & Thornhill, B. A. Ureteral obstruction as a model of renal interstitial fibrosis and obstructive nephropathy. *C.<)#4$5)37* &", 1145-1152,(2009).

7 Yang, H. C., Zuo, Y. & Fogo, A. B. Models of chronic kidney disease. *?('/$?.20&6$!&<*4$?.2$E&<#+2* &, 13-19,(2010).

8 Caplin, B. & Leiper, J. Endogenous nitric oxide synthase inhibitors in the biology of disease: markers, mediators, and regulators? *@(3#(.&20+#(7$!"(&1-7$F*07$G.&+7* %!, 1343-1353,(2012).

For Peer Review